Limitations of Linear Cross-Entropy as a Measure for Quantum Advantage

Xun Gao, 1,2,* Marcin Kalinowski, 1 Chi-Ning Chou, 3 Mikhail D. Lukin, 1 Boaz Barak, 3 and Soonwon Choi 4,†

¹Department of Physics, Harvard University, Cambridge, Massachusetts 02138, USA ² JILA and Department of Physics, University of Colorado, Boulder, Colorado 80309, USA ³ School of Engineering and Applied Sciences, Harvard University, Cambridge, Massachusetts 02138, USA ⁴Center for Theoretical Physics, Massachusetts Institute of Technology, Cambridge, Massachusetts 02139, USA



(Received 28 January 2022; revised 24 July 2023; accepted 20 November 2023; published 29 February 2024)

Demonstrating quantum advantage requires experimental implementation of a computational task that is hard to achieve using state-of-the-art classical systems. One approach is to perform sampling from a probability distribution associated with a certain class of highly entangled many-body wave functions. It has been suggested that such a quantum advantage can be certified with the linear cross-entropy benchmark (XEB). We critically examine this notion. First, we consider a "benign" setting, where an honest implementation of a noisy quantum circuit is assumed, and characterize the conditions under which the XEB approximates the *fidelity* of quantum dynamics. Second, we assume an "adversarial" setting, where all possible classical algorithms are considered for comparisons, and show that achieving relatively high XEB values does not imply faithful simulation of quantum dynamics. Specifically, we present an efficient classical algorithm that achieves high XEB values, namely 5-12% of those obtained in the state-of-the-art experiments, within just a few seconds using a single GPU machine. This is made possible by identifying and exploiting several vulnerabilities of the XEB, which allows us to achieve high XEB values without simulating a full quantum circuit. Remarkably, our algorithm features better scaling with the system size than a noisy quantum device for commonly studied random circuit ensembles in various architecture. We quantitatively explain the success of our algorithm and the limitations of the XEB by using a theoretical framework, in which the dynamics of the average XEB and fidelity are mapped to classical statistical mechanics models. Using this framework, we illustrate the relation between the XEB and the fidelity for quantum circuits in various architectures, with different choices of gate sets, and in the presence of noise. Taken together, our results demonstrate that XEB's utility as a proxy for fidelity hinges on several conditions, which should be independently checked in the benign setting, but cannot be assumed in the general adversarial setting. Therefore, the XEB on its own has a limited utility as a benchmark for quantum advantage. We briefly discuss potential ways to overcome these limitations.

DOI: 10.1103/PRXQuantum.5.010334

I. INTRODUCTION

Quantum advantage refers to the experimental demonstration of the computational power of a quantum device far beyond that of any existing classical devices. Such demonstration is important because it not only constitutes a milestone of quantum technology, but also challenges the so-called extended Church-Turing thesis [1,2], which has been central to computational complexity theory. A straightforward way to demonstrate quantum advantage would be to explicitly run a quantum algorithm, such as Shor's integer factoring [3], for problems whose size is too large (e.g., 2048-bit integers) to be solved by any known algorithm running on classical computers. However, this would require a quantum device with a large number of near-perfect qubits, which is well beyond the capabilities of the existing technology. State-of-the-art quantum devices consist of several dozens of imperfect qubits [4-9]. Even the exploration of a potential scaling advantage requires larger systems, consisting of at least several hundred coherent qubits.

Instead of implementing such quantum algorithms, most of the current efforts towards demonstrating quantum advantage have focused on sampling problems [10–12], which are well suited for near-term quantum devices [5– 7,13,14]. In these problems, one is asked to produce a sequence of random bitstrings drawn from a certain probability distribution. A natural choice of a distribution

^{*}Xun.Gao@colorado.edu †soonwon@mit.edu

Published by the American Physical Society under the terms of the Creative Commons Attribution 4.0 International license. Further distribution of this work must maintain attribution to the author(s) and the published article's title, journal citation, and DOI.

that would be challenging for a classical computer to reproduce is one based on a highly entangled many-body wave function. Indeed, it has been shown [2,15–22] that, for a wide class of quantum states, exact sampling by classical computers is intractable under plausible assumptions [2,15,16,22–27].

To demonstrate quantum advantage using an actual sampling experiment, one needs to introduce a benchmark that measures how close the sampled distribution q(x) of a quantum device is to the (ideal) target distribution p(x). The idea is that on one hand, one shows that the samples from the quantum device achieve high values (indicating good correlation with the ideal distribution), while on the other hand, one presents evidence that there does not exist an efficient classical algorithm that can produce samples achieving comparable values. If the difference between the classical and quantum resources needed to achieve a certain value of the benchmark scales exponentially with the system size, this demonstrates that quantum devices have an exponential computational advantage even in the regime where the gates are too noisy to allow for quantum error correction. A prominent example of such a benchmark is the *linear cross-entropy benchmark* (XEB) [5] defined as

$$\chi_p(q) = 2^N \sum_{x \in \{0,1\}^N} p(x)q(x) - 1. \tag{1}$$

Intuitively, $\chi_p(q) > 0$ if q places more mass on the elements x whose probability is higher than the median in p. A nonvanishing value of $\chi_p(q)$ is taken to mean that the sampled distribution is correlated with the ideal one. A crucial difference compared to *fidelity*,

$$F = \langle \psi | \rho | \psi \rangle,$$

is that the XEB is defined using only measurements in the computational basis, namely $p(x) = |\langle x|\psi\rangle|^2$ and $q(x) = \langle x|\rho|x\rangle$, where ρ is the quantum state produced by a physical noisy quantum device and $|\psi\rangle$ is the ideal state expected from the quantum circuit without any noise or errors.

The XEB measure has been used in recent experiments [5,6], where sampling from random unitary circuits was performed. Specifically, Google [5] achieved an XEB value of $\chi_p \approx 0.002$ on a two-dimensional, 53-qubit quantum device (Sycamore) implementing circuits up to depth 20 and estimating XEB under reasonable assumptions [28]. Recently, the USTC group [6,7] extended the number of qubits and claimed the XEB value of 6.62×10^{-4} and 3.66×10^{-4} , for system sizes up to 56 qubits and 60 qubits, respectively. In both cases, it has been conjectured that such values are challenging to achieve using state-of-the-art classical computing devices on a realistic time scale.

The motivation for using the XEB as a benchmark is twofold. First, compared to fidelity, the XEB is relatively easy to estimate in an experiment using a small number of samples due to the fact that the variance of XEB is of order unity (see the Supplemental Material of Refs. [5] and [29] for detailed discussions); in contrast, fidelity is intrinsically a many-body quantum quantity such that any classical measurement would lose a certain amount of information and hence in principle one has to estimate as many amplitudes of the quantum state as possible. Other more quantum measurements like the SWAP test [30,31] and the classical shadow [32] are more efficient in terms of the number of samples in principle. However, these measurements require global and/or even coherent quantum operations, which also suffer from noises. Thus it is infeasible to get a reasonable estimation of fidelity for noisy states with intermediate sizes (say more than 50 qubits) in the current experiments. Second, the XEB is believed to be correlated with the fidelity [33]. Therefore, one may expect that achieving a high XEB value implies the demonstration of quantum advantage. However, we emphasize that the nature of quantum advantage experiments must be inherently adversarial: it is not sufficient to show that an experiment achieves a good value on a benchmark—one needs to argue that every possible classical algorithm cannot achieve the same value. Otherwise, certain adversarial classical algorithms may take "shortcuts" and achieve good values on the benchmark, despite not really simulating the target quantum circuit.

To be more specific, the XEB has been used in Refs. [5–7] to simultaneously serve two distinct purposes:

- (1) **Proxy for fidelity:** the XEB is considered as a good approximation to the many-body fidelity $F = \langle \psi | \rho | \psi \rangle$ for chaotic quantum systems [5,18,34–36], where $|\psi\rangle$ is the ideal target state and ρ is the state prepared by a noisy device.
- (2) Certification of quantum advantage: it has been suggested that obtaining bitstring samples with a significant XEB value on a classical device is computationally difficult [37], which would allow XEB to certify quantum advantage.

In this work, we critically assess these roles of XEB and present two major results. First, we characterize the relation between XEB and fidelity in the "benign" setting of comparing a noisy quantum device to an idealized noiseless circuit, showing how this correlation depends on the architecture and the choice of gate sets. Based on these considerations, we identify the conditions under which the XEB can be used as a proxy for the fidelity. Second, we show that the XEB is not a good measure of quantum advantage in the "adversarial" setting, by presenting a classical "spoofing" algorithm that achieves XEB values within around one order magnitude to those

demonstrated in the experiments, using only desktop-scale computational resources within a few seconds. This is possible because our classical algorithm explicitly violates the aforementioned conditions, where the XEB approximates the fidelity.

Prior works challenging quantum advantage [38–43] obtained comparable or higher XEB values using heavy computational resources. While these classical methods are tailored to challenge Google's current setup (53 qubits, depth 20), up to now it was unclear if and how they could be extended to larger systems. In fact, it has been argued that by simply increasing the system size to about 60–70 qubits, one could defeat such classical spoofing algorithms [44]. Indeed, in more recent experiments [7] (60 qubits, depth 24), it has been suggested that the new device bypasses the challenge of these algorithms. In what follows we show that the XEB has a fundamental limitation as a proof of quantum advantage beyond a simple competition arising from the scaling of system sizes.

In particular, we show that XEB values produced by our algorithm feature more favorable scaling with the system size than a realistic, noisy quantum device. As a result, our algorithm is expected to outperform such experiments on average if their architecture is extended to involve more qubits, without a corresponding improvement in average gate fidelities.

Before proceeding, we emphasize that XEB is an efficiently measurable benchmark in which polynomially many samples are sufficient to estimate its value with high precision (although it is computationally inefficient to calculate this estimation). Such efficiently measurable benchmarks are essential for certifying quantum advantage. While fidelity could have been used directly to characterize the performance of quantum circuits, it is inherently a many-body quantum quantity and hence is, in principle, classically intractable. As such, it can not be used to characterize a computational task, i.e., the fidelity cannot be defined for classical algorithms. At the same time, the use of classical probability distance measures (e.g., Bhattacharyya or Hellinger distances, KL divergence, or total variation distance) is challenging since it is difficult to obtain empirical estimates for these quantities from experiments. This is because the domain of these distributions is exponentially large; all of these distances require not just an exponential computation time but also an exponential number of samples to estimate (cf., [45, Chap. 5]), which is impractical.

A. Vulnerabilities of the XEB

In this work, we exploit three distinct properties of the XEB that make it vulnerable against adversarial attacks. First, the XEB and fidelity may diverge from one another

in the presence of errors highly correlated in their spacetime locations. Second, the XEB and fidelity exhibit distinct scaling behavior with increasing system size: when multiple systems are brought together to form a larger one, the XEB generally increases with the number of subsystems, while the fidelity decays exponentially. Finally, the XEB is designed to quantify the amount of correlation between an ideal probability distribution p(x) and an experimentally obtained one q(x), but this correlation can be dramatically amplified if one has direct access to the full description of q(x) (in contrast to only having samples drawn from it). Combining these three properties, one can devise an efficient, adversarial algorithm that achieves high XEB values for state-of-the-art quantum circuit sizes, using computational resources as minimal as a single desktop-scale GPU device. In this work, we demonstrate this approach by introducing a simple classical algorithm. Before presenting our main results, we elaborate on the first two properties of XEB using a heuristic and intuitive analysis; the third—the amplification of correlations—is explained in Sec. IIIB and a similar idea has been already exploited in the prior work [39,40,42,46].

1. Discrepancy of XEB and fidelity

The fact that the XEB approximates fidelity can be intuitively understood using the following simplified analysis [5]. For a noisy circuit in the presence of independent, homogeneously distributed random errors at rate ϵ , the system executes the entire circuit without any error with probability $P_{\text{no err}} = (1 - \epsilon)^{\text{#gates}}$ where #gates denotes the number of gates. If we assume that the presence of a single or more errors leads to vanishing contributions to the XEB or fidelity, both XEB and fidelity equal $P_{\text{no err.}}$ While this argument can be made rigorous in appropriate limiting cases, the exact relation between the XEB, fidelity and $P_{\text{no err}}$ involves nonzero correction terms for finite-size systems with finite error rates. See the Supplemental Material [47] for a more detailed discussion and a qualitative derivation; here we provide only the outline of our argument. For example, let us consider the effect of a single bit-flip error \hat{X} , occurring at depth t in a one-dimensional (1D) random circuit evolution, on the value of XEB and fidelity. This effect can be understood in the Heisenberg picture by inspecting the error operator $\hat{X}(t)$, propagated backwards in time, at t = 0, acting on a simple initial state such as $|0\rangle^N$ [see Fig. 1(a)]. In the case of chaotic dynamics, $\hat{X}(t)$ becomes a random linear combination of $4^{|s|}$ Pauli string operators, where the support size of the operator $|s| \approx 2ct$ grows linearly in time with an effective "scrambling" velocity c. Among these Pauli strings, approximately $2^{|s|}$ operators are products of only identity I or Z operators, for which the initial state is an eigenstate, leading to no change in XEB or fidelity. Consequently, even if a single error occurs, it contributes to the XEB

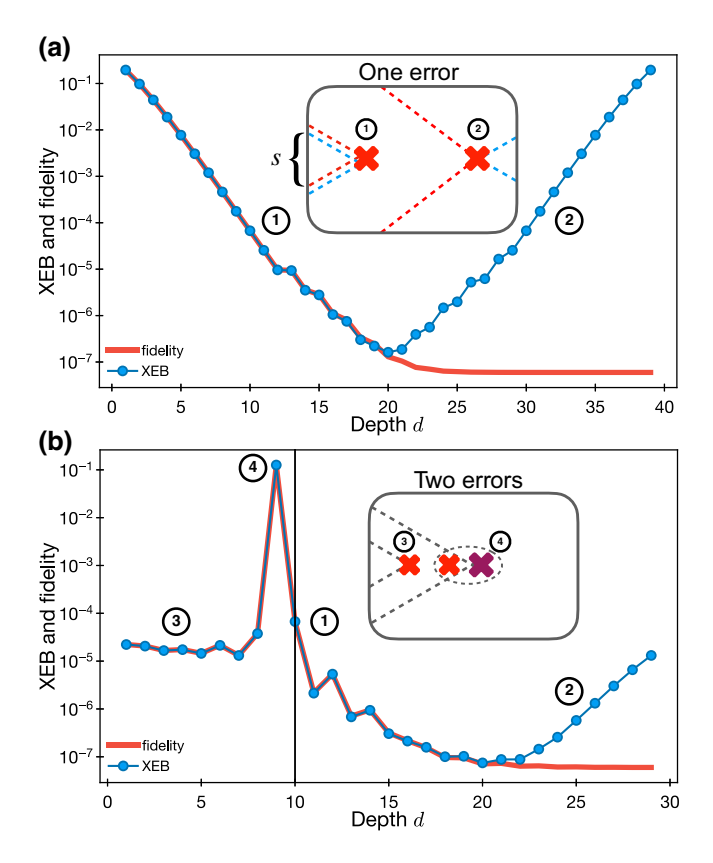


FIG. 1. Effects of a single or double error at various locations on the XEB and fidelity. (a) In the presence of a single error, the XEB and fidelity is reduced to an exponentially small but nonzero value that depends on the location of the error. The scaling of the XEB or fidelity can be understood in terms of the size |s| of the error operator propagated to boundaries in the Heisenberg picture (inset). (b) In the presence of two errors, the XEB and fidelity significantly depend on their relative location: the effect of one error can be masked (marked 3) or even canceled (marked 4) by that of another error.

and fidelity by a small correction $O(2^{-2ct})$. For the case of XEB, a similar argument can be made by propagating the error operator forward to the measurement time because the combination of I and Z operators do not affect measurements in the computational basis, leading to a sharply distinct behavior from fidelity when an error occurs near the measurement time.

Naïvely, these corrections may seem small and unlikely to result in any substantial deviations of XEB and fidelity from $P_{\text{no error}}$. However, compounding the problem is that exponentially many different events give rise to the same amount of corrections when we consider events with multiple errors. For instance, if a second error is added to the system, such that its support is contained within that of the first error [Fig. 1], their net contribution to the correction remains the same because the combined propagated error operator is still a random linear combination of Pauli operators. In fact, one can add any number of errors within

the lightcone of the first one without decreasing the net correction term. Therefore, a substantial, nonperturbative correction may arise from a family of error events, where multiple errors are clustered at early (late) times for both XEB and fidelity (for XEB). Even when errors occur deep inside the circuit, the effects of two consecutive errors may cancel each other with probability approximately 1/10 [Fig. 1(b)], leading to a contribution of order unity to the fidelity and the XEB. We provide more details on this high-level picture in Secs. II A, II B, and II C within the Supplemental Material [47].

Based on this analysis, one can provide an approximate lower bound on total correction by summing over a few classes of error configurations [47]. Assuming that errors are independent and homogeneously distributed over the whole system (benign setting), we find that it is necessary and sufficient conditions for XEB, fidelity, and $P_{\text{no error}}$ to agree one another $N \in f(c) \ll 1$, where f(c) is a decreasing function of order unity that depends on the microscopic details and the architecture of a quantum circuit [47]. Recent experiments [5–7] approximately satisfy this condition, and we expect that XEB values would overestimate fidelities only by a few percents [48]. We emphasize that this conclusion requires the independence of errors over space and time that needs to be explicitly checked. In the presence of correlated errors (corresponding to adversarial setting), the corrections to XEB and fidelity may dominate their entire values, even if the total error rate remains small. This can be seen from the example in Fig. 1(b): if the errors are correlated such that their position is distributed over a relatively small region, the effects of overlapping lightcones and error cancelation could be strong, leading to potentially large (compared to $P_{\text{no error}}$) corrections to the XEB and fidelity. In particular, if the errors occur in a region near the output boundary, the fidelity is suppressed due to a large lightcone (red in Fig. 1) while the XEB is affected only by much smaller overlapping lightcones (blue in Fig. 1), leading to the discrepancy between the XEB and the fidelity. Contrarily, if the errors are uncorrelated, the lightcones contributing to the XEB do not overlap, and collectively suppress the XEB value such that it is similar to the fidelity. Based on these observations, we design an algorithm that allows for efficient classical simulation, while the discrepancy between the XEB and the fidelity is significantly amplified compared to the benign setting.

2. Scaling of XEB and fidelity

XEB and fidelity exhibit different scaling behaviors when a system size is increased with a fixed error rate, implying that two quantities cannot agree in a certain scaling limit. While a rigorous analysis can be made using the framework presented in Sec. IV, here we consider a toy model illustrating the origin of the different scaling behaviors. Let us consider *k* disjoint *N*-qubit systems,

each undergoing noisy circuit evolution with corresponding XEB values $\chi_i = 2^N \sum_x p_i(x) q_i(x) - 1$ and fidelities F_i with $i = 1, 2, \ldots, k$. Here $p_i(x)$ and $q_i(x)$ are bitstring probabilities for ith quantum system obtained from an ideal circuit and from noisy dynamics (or any other classical algorithms), respectively. If we consider the k disjoint systems as a single composite system of kN qubits, one can explicitly check that the fidelity scales multiplicatively, i.e., $F_{\text{total}} = \prod_i F_i$, while the XEB additively:

$$\chi_{\text{total}} = 2^{kN} \sum_{\{x_i\}} \prod_i p_i(x_i) q_i(x_i) - 1$$

$$= \prod_i \left(2^N \sum_{x_i} p_i(x_i) q_i(x_i) \right) - 1$$

$$= \prod_i (\chi_i + 1) - 1 \approx \sum_i \chi_i,$$
(3)

where the second equality is due to the product structure across the subsystems and we assumed that $\chi_i \ll 1$ in the last line, relevant for the regime of our interest. While this example may seem contrived as each subsystem is perfectly isolated, one can also devise an example, where all subsystems are strongly coupled by unitary gates and result in fully globally scrambled quantum states.

This discrepancy in scaling stems fundamentally from the structure of the XEB formula in Eq. (1): as two distributions p(x) and q(x) become uncorrelated [49] from one another, the first term in Eq. (1) tends to a finite value,

1, rather than approaching zero. This offset is explicitly subtracted in order to obtain a value within an interval [0, 1], but it also leads to distinct scaling behavior for large composite systems.

B. Main results

Our key results can be summarized as follows. More details about the assumptions and scope of the results will be provided in the relevant section and see Sec. I within the Supplemental Material for a summary [47]. First, we present a simple and efficient classical algorithm to spoof the XEB measure. In particular, we show that as the number of qubits increases, the performance of our algorithm scales *better* on average than that of a noisy quantum simulation in a number of practical settings (see Fig. 2). Hence, the XEB does *not* constitute a scalable measure to certify quantum advantage. Second, we develop a new theoretical framework to analyze and predict the XEB under various choices of quantum circuit architectures and gate ensembles. This framework allows us to understand the relation between the XEB and the fidelity (see Fig. 3).

1. Classical algorithm spoofing XEB

Our algorithm is inspired by the observation that entanglement growth in a noisy quantum circuit is reduced by errors spread over the entire circuit in both space and time [Fig. 2(a)]. These effectively truncate entanglement and correlations among different subsystems. In our algorithm, we introduce a similar amount of effective errors, but they

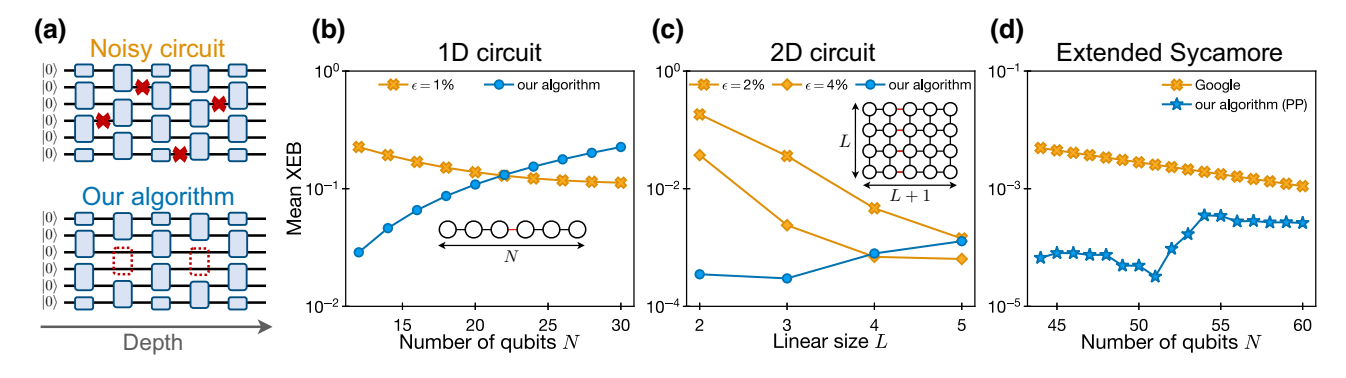


FIG. 2. Classical algorithms spoofing XEB for quantum circuits in various architectures. (a) Schematic diagrams illustrating the key idea of our algorithm. In noisy quantum circuits, errors (red crosses) randomly occur at a rate $\epsilon > 0$, spread over the entire circuit. In our algorithm, we introduce effective, highly localized errors by omitting or modifying a few entangling quantum gates (red dotted boxes) such that the circuit splits into smaller segments and becomes easier to simulate classically. (b)–(d) Performance of our algorithm. We obtain high XEB values (blue circles and stars) compared to noisy circuits (yellow crosses and diamonds) for 1D, 2D, and the extended Sycamore circuit architectures [see Fig. 5]. (b) 1D circuits of depth d=16 in the brick-work layout, with the Haar random two-qubit gate ensemble. (c) 2D circuits of depth d=16 in a $L \times (L+1)$ square lattice, with the Haar random two-qubit gate ensemble. Our algorithm outperforms noisy quantum circuits (here with error rates $\epsilon=0.02$, 0.04) for sufficiently large system sizes. Insets in (b),(c) show the circuit architecture and the position of omitted gates (red lines). (d) Comparison of the mean XEB value obtained by our improved algorithm (light blue circles) to Google's Sycamore in which case we extrapolated experimental results using the ansatz XEB $\sim \exp(-c_1N - c_2Nd)$. We extended the Sycamore architecture horizontally up to 60 qubits; see Fig. 5 for more details. For this simulation, we assumed a quantum circuit ensemble with random single-qubit gates similar to (but slightly modified) those used in Ref. [5–7] [see Sec. III C].

occur only at specific locations such that the quantum circuit becomes easier to simulate. As an example, Fig. 2(a) shows how omitting a few specific gates at certain locations (which amounts to particular types of error, i.e., *gate defects*) can split a circuit into multiple disconnected subcircuits. Alternatively, one can apply a completely depolarizing channel before and after an entangling gate. These approaches explicitly remove correlations between subsystems. Intuitively, when the amount of "effective noise" in a noisy quantum simulation is comparable to the "effective error" in our algorithm (proportional to the number of omitted gates), the XEB of the latter is larger due to the stronger correlation among errors [see Fig. 1(b)].

Since the size of each subcircuit is much smaller than that of the original circuit, the algorithm can be significantly faster than a direct simulation of the global circuit. In particular, when ran on 53-qubit circuits, such as Google's, it takes a few seconds using a single GPU (32GB NVIDIA Tesla V100). The existence of our classical algorithm has three types of implications:

- (1) Complexity-theoretic implications: a linear-time classical algorithm that outperforms any noisy 1D quantum circuit. For one-dimensional quantum circuits consisting of Haar random unitary gates, we present a linear-time classical algorithm, which achieves higher XEB values than noisy quantum devices. Concretely, for every uncorrelated error rate $\epsilon > 0$ per gate, our algorithm can spoof the XEB measure when the number of qubits is sufficiently large. Here, uncorrelated error refers to errors from different locations being uncorrelated, i.e., the error channel is a tensor product of error channels of each location.
- (2) Experimental implications: a highly efficient classical algorithm (1 GPU around 1s), whose performance is within around one order of magnitude with current experimental devices. We consider a random circuit ensemble modeled after the one used in Ref. [5–7] (see Sec. III C and Ref. [47] for detailed information). Our algorithm achieves a mean XEB value that is about 8% of Google's experiment (53 qubits, depth 20), and 12% and 2% of USTC's experiments (56 qubits, depth 20 and 60 qubits, depth 24), respectively, with the running time approximately equal to 1 s using 1 GPU. We can get higher XEB value by taking more running time. For example, 12.3% of Google's experiment with 50 s and 5% of USTC's second experiment with 4 s.
- (3) **Scaling implications:** remarkably, the XEB value of our algorithm generally *improves* for larger quantum circuits, whereas that of noisy quantum devices quickly deteriorates. Such scaling continues to hold when the number of qubits is increased while the depth of the circuit and the error-per-gate are fixed,

as explicitly confirmed from numerical simulations for 1D and two-dimensional (2D) square and the extended Sycamore architecture in Figs. 2(b)–2(d).

Crucially, we show that a classical algorithm can obtain high XEB values even when the corresponding fidelity is very low. This implies that *high values of XEB cannot certify quantum advantage*. Even if one estimates the fidelity of each individual gate separately and observes good agreement between XEB and the anticipated circuit fidelity, as is the case in Ref. [5–7], this does not necessarily imply high many-body fidelity without additional assumptions such as the independence and the homogeneity of errors. In other words, XEB cannot be used as a "black-box" measure for certification.

2. Understanding XEB and circuit fidelity via mapping to a statistical mechanics model

We present a way to analyze quantum circuit dynamics using classical statistical physics. Specifically, for a wide class of random circuit ensembles involving single-qubit Haar random gates, we show that the dynamics of both noisy quantum circuits and our classical algorithm can be understood in terms of an effective diffusion-reaction process, which was originally used to study the scrambling of circuits [50]. In this effective description, the application of each layer of a quantum circuit translates to particles undergoing a random walk (diffusion) for a single time step on a graph representing the circuit architecture. Furthermore, each particle can duplicate itself, and a pair of particles may recombine into a single particle at a certain rate (reaction). The rates of particle diffusion and reaction are determined by the properties of two-qubit quantum gates, such as the average amount of entanglement they generate. The XEB and the fidelity of ideal circuits are given by different aspects of particle distribution at the last circuit layer, as we elaborate in Sec. IV C.

The XEB value in a noisy circuit and our algorithm will decrease from the ideal value when a particle hits a defective (omitted or noisy) gate. In the case of noisy quantum circuits, every gate is noisy, so the decrease in the XEB value is proportional to the total number of particles in the diffusion-reaction process. Intuitively, when the system size grows, there are more particles hitting noisy gates and thus the XEB value becomes smaller. In our algorithm, the XEB decreases whenever a particle hits an omitted gate at the boundaries of disconnected subregions. Intuitively, when the system size grows, there is more space for particles to diffuse away from the boundary and thus, in general, the XEB value can become larger. This qualitatively explains the asymptotic scaling of XEB in Fig. 2.

The mapping to diffusion-reaction models can also help explain the XEB's role as a proxy for the fidelity. As we

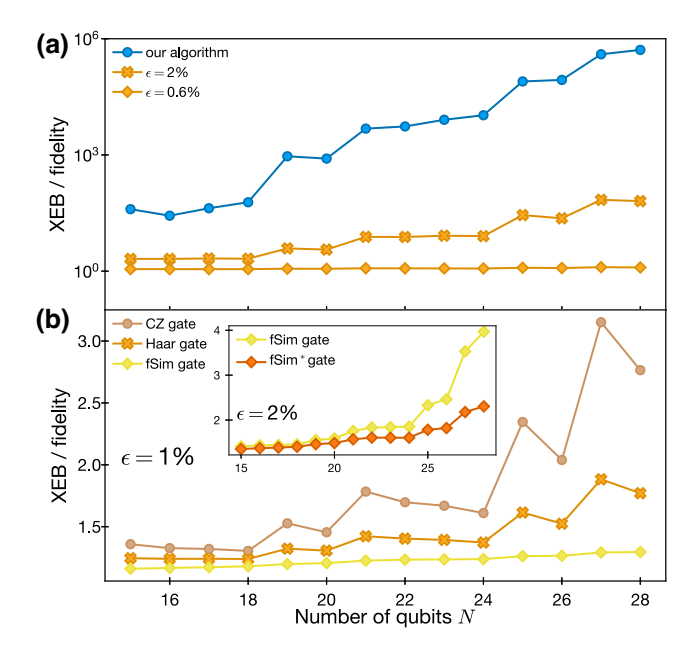


FIG. 3. The ratio between XEB and fidelity evaluated for quantum circuits of depth 20 in Sycamore architecture for various system sizes [according to the qubit ordering in Ref. [5]; see also Fig. 10(a)]. (a) The ratios for our algorithm (blue) are much larger than those for noisy circuits (yellow), shown with two different error rates, despite the fidelity being lower in the former case. The local gate ensemble is 2-qubit Haar. (b) The ratios for noisy circuits with various types of gate ensembles. Out of the three standard gates (CZ, Haar, fSim with Haar random single-qubit gate), the discrepancy between the XEB and fidelity is minimized in circuits with the fSim ensemble. Following on the insights from our theoretical analysis, we propose a new gate: $fSim^*$, which corresponds to the $fSim_{\theta,\phi}$ from Eq. (5) at $(\theta, \phi) = (90^{\circ}, 0^{\circ})$, and produces the smallest possible discrepancy between the XEB and the fidelity (see Sec. IVB). (Inset) Comparison between the usual fSim gate and the new fSim* gate.

elaborate in Sec. IV C, the XEB and the fidelity agree with each other if and only if the particle distribution at the last circuit layer reaches a certain homogeneous, steady-state profile. Both in noisy circuits and in our algorithm, the final distribution is modified by particles hitting defective gates, leading to the discrepancy between the XEB and the fidelity.

In our algorithm, the deviation from the target distribution is induced by the presence of omitted gates located along boundaries of disconnected subsystems, which leads to a strong violation of the homogeneity of the particle distribution. Therefore, XEB and fidelity are very different in this case. On the other hand, in noisy circuits, the particles hit defective gates uniformly across the system, and thus the homogeneity is retained. This results in a small discrepancy between XEB and fidelity, especially in the weak-noise regime [see Fig. 3(a)].

For noisy chaotic systems, it is believed that faster scrambling leads to a better agreement between XEB and

fidelity [4,5,35,36]. In the diffusion-reaction model, the reaction rate and the diffusion rate are related to the scrambling speed and the above-mentioned intuition is reflected in a faster approach to the steady state for rapid mixing. Compared to several other commonly studied two-qubit gates, like the control-Z and Haar-random gates, the fSim gate used in Google's experiment has a similar reaction rate but a faster diffusion rate. Therefore, it produces the smallest discrepancy between XEB and fidelity among these gates. However, the fSim gate is still not the optimal choice. By increasing the reaction rate further, we find the optimal gate, which we call fSim* due to its similar structure; see the inset of Fig. 3(b) for the comparison between fSim and fSim*.

The choice of the single-qubit ensemble can also affect the diffusion-reaction processes of particles. In particular, we find empirically that Google's choice of single-qubit gates, which maps both computational basis states, e.g., $|0\rangle$ and $|1\rangle$, to their equal superposition with opposite phases, leads to significantly faster diffusion-reaction processes and makes our algorithm relatively less effective.

In the case of one-dimensional circuits with Haar random gates, a more detailed scaling analysis is possible by mapping a quantum circuit to a two-dimensional classical Ising model [51-57], which can be regarded as a special case of the diffusion-reaction model. In the case of ideal circuits, the classical model exhibits the \mathbb{Z}_2 Ising symmetry. However, when noisy processes or gate defects are introduced, they appear as effective external magnetic fields, which break the Ising symmetry. In this picture, the deviation of the XEB from unity characterizes the degree of symmetry violation [56]. Crucially, the noise and omitted gates have distinct effects, appearing as bulk and boundary fields, respectively. In the limit of large circuits, the bulk field has a stronger effect than the boundary field, even when the strength of the bulk field is vanishingly small. Closely related to spontaneous magnetization in the ferromagnetic phase, this phenomenon provides an intuitive explanation for the superior XEB scaling of our classical algorithm, compared to that of noisy quantum circuits.

C. Organization of the paper

The rest of our paper is organized as follows. The next two sections include a summary of the necessary background and a detailed presentation of our results. We review the definition, properties, and applications of the XEB in Sec. II. In Sec. III, we describe our algorithm and random quantum circuit ensembles in more detail, and summarize our results and their implications. We discuss related works on the XEB spoofing in Sec. III D. Then, we introduce the technical aspects of mappings to statistical physics models: the diffusion-reaction model in Sec. IV B, with the detailed discussion of the relationship

between the XEB and the fidelity in Sec. IV C, and the Ising model for 1D circuits with the Haar gate ensemble in Sec. IV D. Finally, we conclude in Sec. V, where we discuss several potential ways to overcome the vulnerabilities of the XEB and present a few interesting future directions. We defer the discussion of the technical details of the heuristic analysis and the diffusion-reaction model, as well as the description of our improved algorithm, to the Supplemental Material [47].

II. LINEAR CROSS-ENTROPY BENCHMARK

We first review the definition of the XEB and its properties, formally introduce the XEB test, and establish our notations.

A. Linear cross-entropy

The XEB corresponds to the linearized version of the cross-entropy (i.e., the quantity $-\sum_x q_x \log p_x$, also known as the log likelihood), which is commonly used to characterize the closeness between the data and target distributions [58]. The motivation to adopt the linearized version is to minimize statistical fluctuation [5,29] when estimating the XEB empirically. Both versions can be used to estimate the fidelity under common error models [5] for sufficiently chaotic circuits, or (equivalently) sufficiently deep random circuits [59]. It is generally believed that simulating complex quantum systems with high fidelity is classically intractable, and so obtaining high XEB values is (naïvely) expected to be hard as well.

Let U be an N-qubit unitary, and let p_U be the probability distribution induced by measuring $U|0^N\rangle$. If q is a probability distribution over $\{0,1\}^N$ then the XEB value of q with respect to U is

$$\chi_U(q) = \chi_{p_U}(q) = 2^N \sum_{x \in \{0,1\}^N} q(x) p_U(x) - 1.$$

If q is uncorrelated with p_U , $\chi_U(q) = 0$ [5,18]. On the other hand, $\chi_U(q) \approx 1$ if q is similar to p_U for random-enough deep circuits, where we expect p_U to be characterized by the Porter-Thomas distribution. Therefore, $\chi_U(q)$ serves as a proxy to estimate how p and q are correlated with one another.

We will often consider the unitary U to be a random variable sampled from a *distribution* over N-qubit unitary transformations that correspond to choosing a circuit with random gates from a prescribed architecture. In this case, the quantity $\chi_U(q)$ is a random variable, and we denote its expectation value over different U by $\langle \chi_U(q) \rangle_U$.

1. Empirical versus expected XEB value

The XEB value for a given circuit U can be empirically estimated with a relatively small number of samples,

compared to its nonlinear counterpart, using an unbiased estimator $\tilde{\chi}_{pU}(q) = 2^N/m \sum_{i=1}^m p_U(x_i) - 1$, where $x_1, x_2, \dots x_m$ are m independent samples obtained from q(x), which can be sampled in practice. In particular, the error $|\tilde{\chi}_{p_U} - \chi_{p_U}|$ scales as approximately $1/\sqrt{m}$. As it is known from previous works [5,29] that the STD of XEB is O(1), the required number of samples scales as $1/\tilde{\chi}_p^2$, which is independent of the system size. Since U is sampled from an ensemble, $\chi_U(q)$ is effectively also random, when m tends to infinity. Therefore, in practice, it is common to take another empirical average $\langle \chi_U(q) \rangle_U$ over K independent circuits U_1, \ldots, U_K . For example, in Google's experiment [5], they choose $m \approx 7 \times 10^6$ and K = 10; in USTC's two experiments [6], they choose $m \approx 1.9 \times 1.9$ $10^7, K = 10$, and $m \approx 7 \times 10^7, K = 12$, respectively. To get a high confidence in the estimation of $\langle \chi_U(q) \rangle_U$, the number of repetitions K should be chosen proportionally to the square of the inverse of the standard deviation (STD) of $\chi_U(q)$.

2. Standard deviation

In the body of this work, we focus on the average value of the XEB, while the statistical fluctuation of empirical estimation is ignored. However, because we are dealing with random circuit ensembles, it is important to control the STD of the classical algorithm's output. More discussion of the STD in various settings is presented within the Supplemental Material [47].

3. Classical and noisy quantum simulations

Let C be a classical randomized algorithm that takes as an input a classical description of an N-qubit unitary U and allows us to sample an N-bit string $x \in \{0,1\}^N$ as outputs with probability distribution $q_{C(U)}$. We define the XEB value of C with respect to U as $\chi_U(C) := \chi_U(q_{C(U)})$. We will use \mathcal{N}_{ϵ} to be a *noise operator* such that $\mathcal{N}_{\epsilon}(U)$ corresponds to applying an ϵ -noisy simulation of U. We will model the noise as independent single-qubit noise, which can be depolarizing or amplitude-damping, see Sec. IV B. We denote by $\chi_U(\mathcal{N}_{\epsilon})$ the XEB value of the distribution of the noisy circuit $\mathcal{N}_{\epsilon}(U)$, applied to $|0^N\rangle$, with respect to the ideal distribution induced by measuring U $|0^N\rangle$.

4. Quantum advantage via XEB

The demonstration of quantum advantage consists of designing a task that can be performed on a physical quantum device, while being intractable for all polynomial-time classical algorithms. One such task, which has been proposed recently, is to achieve a high XEB value [5,37]. In this scenario, in order to demonstrate quantum advantage using an ϵ -noisy quantum simulator, we need to come up with a probability distribution U over quantum circuits such that for every efficient classical algorithm C,

 $\chi_U(\mathcal{N}_{\epsilon}) \gg \chi_U(C)$ with high probability over the randomness of U. To make the comparison between $\chi_U(\mathcal{N}_{\epsilon})$ and $\chi_U(C)$ rigorous, we need to specify the parameters of the quantum device, such as the number of qubits N and the noise strength ϵ . In the theoretical and asymptotic setting, we pick an arbitrarily small constant $\epsilon > 0$ and consider the relation between $\chi_U(\mathcal{N}_{\epsilon})$ and $\chi_U(C)$ when N tends to infinity and C ranges over all polynomial-time classical algorithms. In practice, we use values N and ϵ that are experimentally achievable. As an example, Google's quantum simulator [5] uses N = 53 and the value of ϵ is empirically estimated to be less than 0.5% [60].

5. Computational hardness of achieving high XEB values

As mentioned previously, when the circuit architecture and gate ensemble are chaotic enough without any noise or error, $\chi_U(U) = \chi_U(\mathcal{N}_0(U)) \approx 1$ for almost all U. In the presence of noise $(\epsilon > 0)$, the distribution $\mathcal{N}_{\epsilon}(U)$ is expected to approach the uniform distribution exponentially in the depth of the circuit; thus, $\chi_U(\mathcal{N}_{\epsilon})$ goes to 0 exponentially in the depth of the circuit as well. Nevertheless, when the quantum circuit size is finite and the strength of noise is sufficiently small, a noisy quantum simulation could achieve nonvanishing XEB value that implies statistical correlation between sampled and ideal distributions. For example, an XEB value of 2.24×10^{-3} in 53-qubit and depth-20 2D circuits was achieved in Ref. [5]. In Ref. [6,7], XEB values of 6.62×10^{-4} and 3.66×10^{-4} were achieved in 56-qubit circuits of depth-20 and 60-qubit circuits of depth 24, respectively.

There are two types of arguments for the difficulty of achieving an XEB value $\chi_U(C)$, using a classical algorithm C, that is bounded away from zero. The first argument, put forward in Ref. [5], was based on the conjecture that brute-force simulation is the optimal classical approach. This conjecture was recently refuted [38–43]. The other, more subtle argument, relies on conjectures in computational complexity.

Aaronson and Gunn [37] reduced the classical hardness of spoofing the XEB measure to the linear cross-entropy quantum threshold assumption (XQUATH), which is a stronger version of the quantum threshold assumption (QUATH) [23]. Our results refute XQUATH assuming the single-qubit gates are Haar random. See more details in Sec. III D and the Supplemental Material [47].

III. SPOOFING ALGORITHMS

We now describe an efficient classical algorithm C that, in a wide range of physically relevant situations, produces a probability distribution with XEB values larger or comparable to that of an ϵ -noisy circuit, at least on average. In such situations, the existence of our algorithm suggests

XEB on its own is not a good benchmark for certifying quantum advantage.

We first describe our algorithm at a high level, deferring its detailed analysis and discussion to Sec. III C. The intuition behind our algorithm borrows ideas from the following observation on noisy simulation of quantum circuits. In a quantum simulation, the presence of noise can remove entanglement and other correlations (either quantum or classical) within the system. Namely, different parts of the system are approximately decoupled. In our algorithm, we compete with an ϵ -noisy quantum simulation by trying to "rearrange" the same amount of total noise in the most favorable way to reduce the computational complexity. This will also allow us to obtain relatively high XEB values owing to its vulnerabilities explained in Sec. I.A. Specifically, we do so by dividing the quantum circuit into isolated subsystems that can be each simulated independently at much lower cost; see Fig. 4 for an example

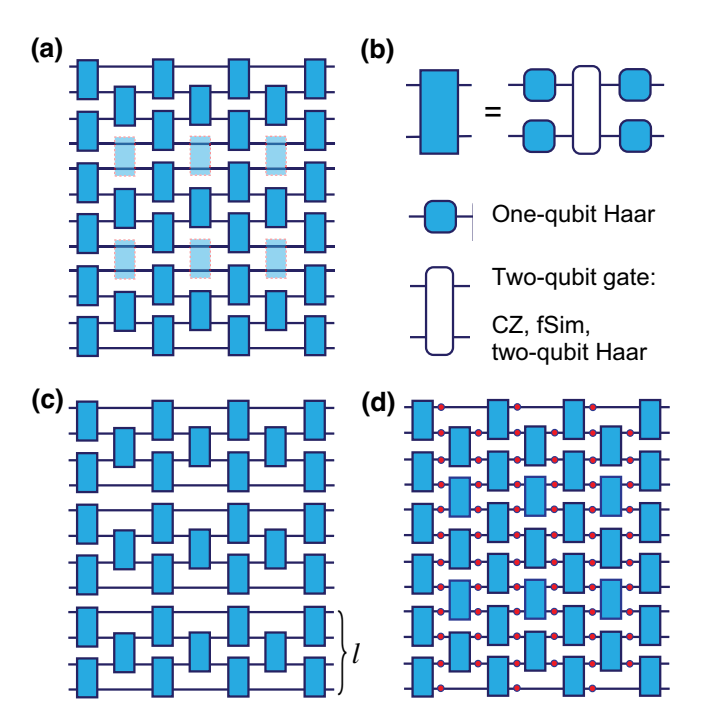


FIG. 4. Illustration of our algorithms. (a) The target (ideal) circuit to simulate. The light blue gates correspond to the ones omitted in (c). (b) Each random two-qubit gate in our circuit consists of any (potentially fixed) two-qubit gate surrounded by four single-qubit Haar random gates. When compared to experimental data, the single-qubit random gates are chosen to be a slight modification of those used in Ref. [5–7]. (c) Our algorithm: one can approximately simulate the ideal circuit by simply omitting a certain subset of gates (in light blue color with red dashed boxes) in the ideal circuit (a). Then, the circuit separates into isolated subsystems. We denote the maximal size of a subsystem as *l*. (d) Noisy circuit: we model the dynamics of noisy quantum circuits by applying probabilistic single-qubit noise (e.g., depolarizing or amplitude damping) channels to all qubits, after each layer of unitary evolution.

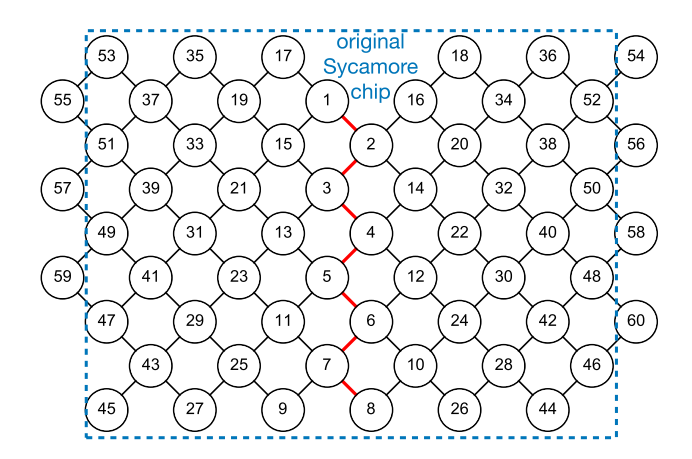


FIG. 5. Sycamore circuit architecture from Ref. [5] and its horizontal extension. The gates marked with red lines are omitted in our algorithm. The Zuchongzhi architecture is very similar; see Refs. [6,7] for more detail.

of a 1D circuit, and Fig. 5 for a 2D circuit). Intuitively, using a similar amount of noise "budget" guarantees that our algorithm achieves a better XEB value comparable to the noisy quantum simulation, while (classically) simulating the smaller isolated subsystems will be exponentially faster than simulating the original circuit. The above explanation is very qualitative and glosses over some important aspects. In Sec. IV C, we give a more quantitative analysis to motivate our algorithm based on the mapping to the diffusion-reaction model.

A. Basic algorithm

We now describe our classical algorithm. For concreteness, we illustrate our algorithm using 1D quantum circuits although it is straightforward to generalize it to other circuit architectures. Let N be the total number of qubits, d be the depth, and l be the maximum size of subsystems [see Fig. 4(a) for an example with N = 12, d = 7, and l = 4]. We start by partitioning the N qubits into subsystems of size at most l by omitting any gates acting across two different subsystems [see Fig. 4(c)]. We then simulate each subsystem separately. Using brute-force methods, simulating a subsystem of l qubits takes at most $2^{O(l)}d$ time. There are $\lceil N/I \rceil$ subsystems and hence the total running time of our algorithm is at most $2^{O(l)}/(l)Nd$. In particular, if l is fixed and does not scale with the total system size N or depth d, the time complexity is linear in the circuit size Nd. We claim that the bitstring distribution induced by the factorizable wave function obtained from our algorithm achieves relatively high XEB values.

B. Improving the algorithm

While our basic algorithm is simple and relatively straightforward to implement, it already has significant consequences for the computational hardness of obtaining high XEB values. Moreover, its practical performance can be further improved via the following modifications.

1. Top-k postprocessing method

Given the output distribution $q_C(U)$ produced by our algorithm C, which is correlated with the ideal distribution $p_U(x)$, it is possible to amplify such correlations by using the so-called *top-k postprocessing heuristic*. In this method, one modifies the bitstring distribution $q_C(x)$ by ordering the bitstrings $x_i \in \{x\}$ from largest $q_C(x_i)$ to the smallest, selecting first k of them (or equivalently setting the probability of the others to 0),

$$q_C(x_i) \to \tilde{q}_C(x_i) = \begin{cases} 0 & \text{if } i \le k \\ 1/k & \text{if } i > k \end{cases}$$
 (4)

Since we can efficiently compute the probability distribution $q_C(x)$ produced by the original algorithm, we can also efficiently compute the amplified probability distribution. As an example, we illustrate this algorithm (with slight modification for simplicity) in the case of l=2 and assume it is efficient to get the entire distributions q_1 and q_2 of the two subsystems, respectively. Thus $q_C=q_1q_2$. Then we sort q_1 and q_2 in a decreasing order and enumerate the bitstrings corresponding to k-largest probability value p_1 and p_2 , respectively. Through this procedure, we get k^2 bitstrings from our classical algorithm.

The intuition behind this heuristic can be understood as follows. The XEB is equivalent to evaluating the average of $p_U(x)$ weighted by q(x) up to an unimportant scaling factor 2^N , and a constant -1. If q(x) is modified such that q(x) is increased (decreased) for bitstrings x with relatively large (small) values of $p_U(x)$, then the weighted average will increase. Given that q(x) and $p_U(x)$ are already positively correlated, such behavior is naturally expected for our top-k postprocessing heuristic, at least on average.

In fact, we can prove that the top-k method increases the XEB if its value is positive and the STD over circuit realizations is not too large. The second requirement is necessary to avoid the situation where some occasional x with small p_x but large q_x will be amplified (in another words, "overfitting"). Unfortunately, this second criterion is not satisfied by our basic algorithm where we simply omit gates. This issue, however, can be straightforwardly addressed using the following method.

2. Self-averaging algorithm

In order to decrease the STD, we make a small modification to our basic algorithm: instead of omitting gates, we insert maximal depolarizing noise or equivalently take average over different realizations of our basic algorithm with random single-qubit unitary at the position of omission. This *self-averaging algorithm* guarantees the positivity and small STD conditions. However, the computational

resources required are larger since we need to simulate mixed state evolution. Interestingly, for a certain class of entangling gates (including the one used in recent experiments [5–7]) that exhibit the "maximal scrambling speed" and that hinders the application of our basic algorithm, one can substantially reduce the computational resources needed for such mixed-state simulation. This is possible because for that class of entangling gates the effect of depolarizing noise can be propagated efficiently [see the Supplemental Material [47] for more detail].

3. Combining algorithmic improvements

In Fig. 7, we present the increase of the XEB for the modified version of Google's gate set ensemble by several orders of magnitude after the application of the top-k method on the self-averaging algorithm. While the discussion above is mostly focused on the mean value of the XEB, it is important to show that our result also holds for typical, individual instances of quantum circuits with a high probability. In the Supplemental Material [47], we show that the self-averaging algorithm offers a much better control over the STD, and guarantees the benefit of using the top-k method. Additionally, we show evidence that the STD of the top-k method decreases as $1/\sqrt{k}$.

C. Performance and implications

Now, we present a comprehensive analysis of the performance of our algorithms and its implications. We consider algorithms both with and without the top-k postprocessing heuristic introduced in the previous section. For practical relevance, we focus on 1D and 2D circuit architectures. For 1D circuits, we theoretically and numerically show that our basic algorithm can achieve, in linear time, a higher average XEB value than noisy quantum systems. More specifically, we show that setting subsystem size to be constant [l = O(1)] is sufficient for our algorithm to obtain a higher XEB value than that of ϵ -noisy quantum simulations, for every constant $\epsilon > 0$, for sufficiently large N. This is due to the distinct scaling behavior of the XEB value for noisy circuits and our algorithm; we discuss in detail the origin of this difference in the scaling behavior in Sec. IV D.

For 2D circuits, we consider Google's Sycamore architecture, which has N=53 qubits [5], and we choose $l \approx \lceil N/2 \rceil = 27$ (Fig. 5). We also consider USTC's Zuchongzhi architectures, which have 56 qubits and 60 qubits, respectively, and we choose $l \approx 28$ for both cases (with some qubits being omitted). A subsystem of this size can be simulated by one NVIDIA Tesla V100 GPU with 32GB memory in about 1 s [61,62]. We analyze the performance of our algorithms on circuits constructed from the following different quantum gate ensembles:

CZ ensemble: each random two-qubit gate is composed of the control-Z gate surrounded by four independent single-qubit Haar random gates [see Fig. 4(b)].

Haar ensemble: each random two-qubit gate is a two-qubit Haar random gate.

fSim ensemble: similar to CZ ensemble, but replacing the control-Z gate by the fSim gate, which is defined as

$$fSim_{\theta,\phi} = \begin{pmatrix} 1 & 0 & 0 & 0\\ 0 & \cos(\theta) & -i\sin(\theta) & 0\\ 0 & -i\sin(\theta) & \cos(\theta) & 0\\ 0 & 0 & 0 & e^{-i\phi} \end{pmatrix}, \quad (5)$$

with parameters $\theta = 90^{\circ}$, $\phi = 60^{\circ}$ [5] (denoted as fSim); we also define a new gate fSim*, which has $\theta = 90^{\circ}$, $\phi = 0^{\circ}$.

fSim with discrete one-qubit ensemble: similar to fSim ensemble, but replacing the one-qubit Haar random gate by $Z(\theta_1)VZ(\theta_2)$ where V is chosen randomly from $\{\sqrt{X}, \sqrt{Y}, \sqrt{W}\}$ ($W = (X + Y)/\sqrt{2}$) but the two Vs between two successive layers on the same qubit should be different; and $Z(\theta_i)$ is chosen randomly from $[0, 2\pi)$.

The last ensemble is closely modeled after quantum circuits used in recent experiments [5–7]. The only modification is that, in experiments, the single-qubit rotation angles θ_i ' are not actively controlled, but rather determined by the specific ordering of quantum gates and the qubit specification at hardware level. We expect that this difference does not influence the performance of our algorithm significantly, because we also consider the case where θ_i is chosen randomly from either 0 or π (which corresponds to I or Z operator, respectively). The numerical result shows that the average XEB values for the top-1 method in the two cases are similar: 0.00018 ($\theta_i \in [0, 2\pi)$) and 0.0004 ($\theta_i \in \{0, \pi\}$), respectively, for the Sycamore architecture (53 qubits, 20 depth). Therefore, we argue that the z-rotation part does not influence the XEB value too much.

1. Implications for 1D quantum circuits

We start by discussing the performance of our algorithm on 1D circuits with gates drawn from the Haar ensemble. For the purpose of this section, C denotes either the algorithm introduced in Sec. III A or its self-averaging version described in detail in the Supplemental Material [47]. The self-averaging version has the same average XEB but a smaller STD, at the cost of requiring more computational power. However, we consider constant subsystem size l = O(1); thus, even the self-averaging algorithm runs in the time linear in Nd.

Result 1. (1D circuits with Haar ensemble) For 1D random quantum circuits with gates drawn from the Haar ensemble and depth at least $d > c \cdot \log N$ for some constant c > 0.

(a) for any constant $\epsilon > 0$ and large enough N (roughly $N\epsilon > 1$), we have

$$\langle \chi_U(C) \rangle_U \ge \langle \chi_U(\mathcal{N}_{\epsilon}) \rangle_U$$
 (6)

for both the basic and the self-averaging algorithms. (b) we conjecture that

$$\sqrt{Var(\chi_U(C))_U} \approx \langle \chi_U(\mathcal{N}_{\epsilon}) \rangle_U$$
 (7)

for the self-averaging algorithm (see the Supplemental Material [47]), which is suggested by numerical simulations. Namely, the standard deviation of $\chi_U(C)$ is comparable to its expectation value $\langle \chi_U(C) \rangle_{U}$.

Combined, this yields a linear-time classical algorithm that spoofs XEB for any noisy quantum simulation of 1D circuits with the Haar gate ensemble, when the number of qubits is large enough.

Equation (6) states that the average XEB of our algorithm is at least as large as that of any noisy circuit with a constant noise level $\epsilon > 0$. As mentioned previously, in practice, we would like the conclusion of Eq. (6) to generalize to typical circuits U (not only on average)—this can be guaranteed by showing that the variance of the XEB value is small. This notion is expressed in Eq. (7), which says that the variance is comparable to the expectation value, and hence our algorithm works for typical instances with large probability. Notice that, in the large depth limit, we expect this to hold only for the self-averaging algorithm. When discussing 1D circuits, where the purpose is to provide complexity-theoretic implications, the analysis of the STD concerns only the self-averaging algorithm. See the Supplemental Material [47] for more detailed discussion.

From a technical point of view, our results are derived by showing that the following quantities decay exponentially with the depth of the circuit:

$$\langle \chi_U(C) \rangle_U = O(e^{-\Delta_1 d}),$$

$$\langle \chi_U(\mathcal{N}_{\epsilon}) \rangle_U |_{\epsilon \to 0 \text{ while } N_{\epsilon > 1}} = O(e^{-\Delta_3 d}).$$

Additionally, numerical simulations support the scaling of the STD as

$$\sqrt{\left\langle \chi_U^2(C) \right\rangle_U - \left\langle \chi_U(C) \right\rangle_U^2} = O(e^{-\Delta_2 d})$$

for some constants $\Delta_1, \Delta_2 > 0$ that depend on the subsystem size l and $\Delta_3 > 0$ that depends on the noise level ϵ .

We emphasize that this scaling is unexpected: the decay rate of the expected XEB value achieved by our algorithm

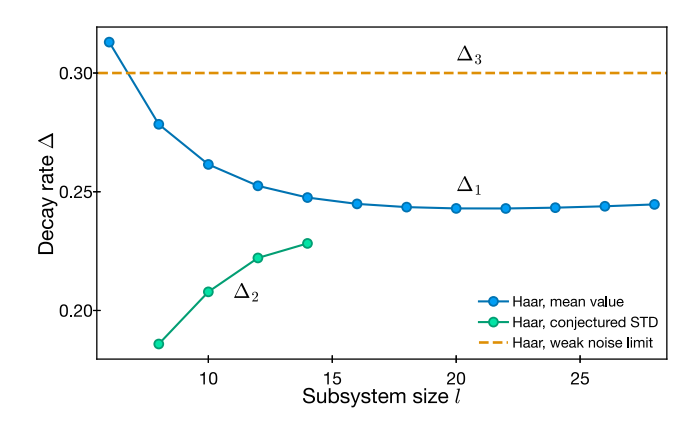


FIG. 6. Exponential decay rates in 1D circuits with the Haar gate ensemble. The mean value (blue) and the standard deviation (green) of the XEB obtained by our algorithm. The horizontal (dashed orange) line is the mean XEB value of the noisy circuit in the weak-noise limit. Intuitively, a smaller Δ corresponds to a larger XEB value. The STD is estimated by an approximate method [47], since the direct calculation is not practical. In the Supplemental Material [47], we give a strong numerical evidence that this approximation is in fact a conservative estimation, i.e., the true STD should be even smaller (Δ_2 should be larger).

does not depend on the system size but only depends on the depth of the circuit. We derive Δ_1 , Δ_3 as constants in Secs. II D and VII B within the Supplemental Material [47]. Numerically, we show in Fig. 6 an estimate on Δ_1 , Δ_2 , and Δ_3 (of 1D circuits with the Haar gate ensemble) with $\epsilon \to 0$ while keeping the system size large enough; in other words, $N\epsilon > 1$. For the Haar ensemble, our numerical results show $\Delta_1 < \Delta_3$, where a larger Δ implies a smaller corresponding quantity in the deep-circuit limit. The numerical calculations suggest that $\Delta_1 \approx \Delta_2$: around l = 14, the gap between the two is very small and Δ_2 (green curve) seems to increase continuously. The green curve is expected to be only a conservative estimation, as explained in the Supplemental Material [47].

2. Implications for quantum circuits in 2D experimentally relevant architectures

Next, we consider 2D quantum circuits in the Sycamore and Zuchongzhi architectures in two different settings. First, we focus on the role of the two-qubit gate, and we analyze the performance of our algorithm for three different two-qubit gate ensembles: Haar, CZ, and fSim. For the single-qubit gate we choose either independent Haarrandom gates, which allows for efficient analysis using the diffusion-reaction model or the more experimentally-relevant discrete gate set. Second, we compare our algorithm against the experimental results of Refs. [5–7]. There, we focus on the fSim gate, and we assume the experimentally relevant discrete single-qubit gate set. These analyses lead to two main results, summarized in

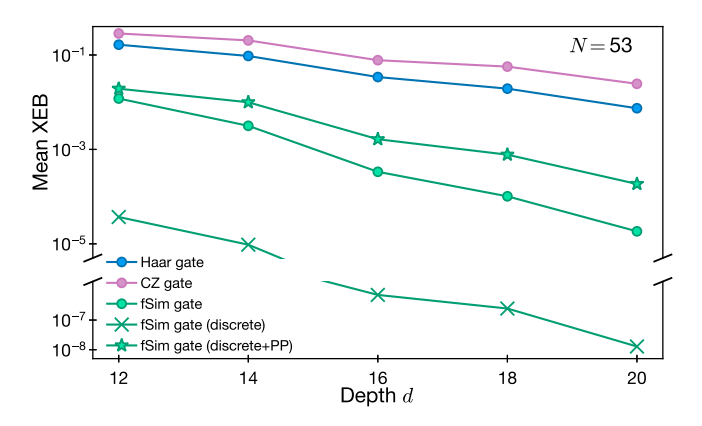


FIG. 7. Mean XEB obtained by our algorithm for different two-qubit gate ensembles, on Google's circuit geometry. Circles denote the Haar single-qubit gate set, while the green crosses (stars) correspond to the more experimentally relevant discrete set (with amplification using the *top-k* method).

Fig. 7 and Table I. For numerical calculations, we used a single GPU machine (32GB NVIDIA Tesla V100).

Result 2. (Different gate ensembles) In the Sycamore architecture with N = 53, d = 20 with Haar-random single-qubit gates, our algorithm (using the partition in Fig. 5) has the following properties:

- (a) the algorithm achieves significant average XEB value for all depths shown in Fig. 7. As a reference, the expected XEB value of a noisy quantum device with depth 20 and error rate $\epsilon \approx 0.5\%$ is approximately equal to 0.002;
- (b) the choice of the two-qubit gate affects the value of XEB, which can be understood in terms of the diffusion-reaction model, Sec. IV;
- (c) the discrete single-qubit ensemble results in much lower XEB values (green crosses in Fig. 7), which is caused by the faster scrambling time;
- (d) the running time (computing the vector of output probabilities) is only 4–8 s.

Result 3. (Comparison with experimental results) For the experimentally relevant gate set (fSim + discrete single-qubit gates) the performance of our algorithm can be summarized (see also Table I) as follows:

- (a) using the top-k postprocessing method, the algorithm achieves average XEB values within around one order of magnitude (approximately equal to 2%–12%) to recent experiments up to depth 20 and 24, respectively;
- (b) the running times (computing the vector of output probabilities and choosing the top-k bitstrings) are on the order of one second;

(c) the STD is conjectured to be comparable to the mean value for large enough k but without decreasing XEB too much; this is supported numerically for Google's Sycamore architecture (see the Supplemental Material [47]).

In summary, our numerical simulations show that our algorithm achieves XEB values within around one order of magnitude to Google's and USTC's circuits in the quantum advantage regime with the experimentally relevant gate set. While our basic algorithm is simple and efficient, there are ways to achieve higher XEB values by adding more sophisticated algorithmic ingredients. For example, we show that after adding a simple postprocessing step (the top-k method), our algorithm can achieve much higher XEB values; for example, compare green crosses and stars in Fig. 7. In fact, we considered only here the most straightforward way to determine the locations of omitted gates (or maximal depolarization noise), which may not be optimal. As we see from Table I, different partitions with roughly the same number of qubits in each part has different XEB values and running time. By generalizing our method, e.g., making the locations of omitted gates (maximal depolarization noise) time and depth dependent, we expect an improved version of our algorithm may produce higher XEB without substantially increasing the computational resources. In this work, we mainly focus on using 1 GPU, which limits the possibilities of partitions. It is interesting to explore using multiple GPUs with better XEB values. In addition, it is an interesting future direction to explore further algorithmic improvements (e.g., adding a modest amount of entanglement).

D. Comparison to prior work

Now, we make a few remarks and compare our algorithm to several previously introduced algorithms that challenged the XEB-based quantum advantage, which utilizes noisy-circuit experiments. First, Ref. [64] proposed an MPS-based approach, which introduces effective "noise" by greedily truncating the entanglement in the system. In that work, the authors consider the CZ gate ensemble and achieve the average XEB value of 0.02, while our approach achieves similar XEB of 0.024 by simply removing the entanglement between two properly chosen subsystems. To achieve the 0.02 XEB value, the algorithm of Ref. [64] requires a runtime of several hours, while our algorithm completes in only 5 min under the same computational resources (1 CPU with 4.5 GB memory). Moreover, Ref. [64] discusses only the effective fidelity and shows that the XEB generally overestimates the fidelity by roughly 10 times. In the present work, we provide a deeper understanding of the connection between the XEB and the fidelity.

TABLE I. The comparison of XEB values (using the top-k postprocessing) and running times in the quantum advantage regime. We find that the average XEB values from our algorithm is largely independent of the choice $k \lesssim 10^4$ (corresponding to more than $k^2 \sim 10^8$ distinct bitstrings for two subsystems), above which they slowly decrease. See the Supplemental Material [47] for the k dependence as well as the estimated STD of XEB values. (a) The running time is measured on a device using 1 GPU (NVIDIA Tesla V100). (b) The performance of our algorithm (XEB value and running time) listed here are measured for the partitions in the Supplemental Material [47], which are not optimized and are chosen for 1-GPU simulation with bounded memory (32GB for our device). In this Supplemental Material [47], we also discuss some other ways to make the simulation more efficient. The tensor network algorithm is based on Ref. [63] and implemented by a Julia package OMEinsum.jl [62].

	Google [5]	USTC-1 [6]	USTC-2 [7]
System size	53 qubits, 20 depth	56 qubits, 20 depth	60 qubits, 24 depth
Claimed running time on supercomputer [7]	15.9d	8.2yr	$4.8 \times 10^{4} yr$
Running time on quantum processor	600 s	1.2 h	4.2 h
Experimental XEB	2.24×10^{-3}	6.62×10^{-4}	3.66×10^{-4}
Running time of our algorithm (1 $GPU^{(a,b)}$)	0.6 s	0.6 s	1.5 s
XEB of our algorithm $^{(b)}$	1.85×10^{-4}	8.18×10^{-5}	7.75×10^{-6}
Ratio of ours to experimental XEB	8.26%	12.4%	2.12%
Running time of our algorithm (a different partition)	50 s		4 s
XEB of our algorithm (a different partition)	2.7×10^{-4}		2.05×10^{-5}
Ratio of ours to experimental XEB (a different partition)	12.3%		5.6%

Another approach is based on tensor network contraction [38,63], which explicitly computes p_x , represented by a tensor network, for as many bitstrings x as possible, and then picks out those x with large values of p_x . Mixing these specially chosen bitstrings with randomly chosen bitstrings forms a set of millions of bitstrings that can spoof the XEB test. Several very recent advances [39–43] are based on a similar idea. In their approach, the computational resources required for simulating only Google's Sycamore chip (53 qubits, depth 20) are either based on supercomputer and massive computer clusters or dozens of GPUs with dozens of hours or days. Because tensor contraction algorithms are inherently exponential in the system size, and hence do not scale to larger systems, spoofing USTC's second experiment (60 qubits, depth 24) is already beyond the scope of the above approach. In contrast, although the XEB values we obtain are not strictly larger than those from experiments, our algorithm only requires 1 GPU with few seconds, and scales better than experiment when increasing system size.

Next, our result for 1D circuits refutes the linear cross-entropy quantum threshold assumption (XQUATH) [37], at least for one of its reasonable modifications, which is a conjecture about the hardness of an approximate counting problem and the hardness of the corresponding XEB-based sampling problem can be reduced to it. In the Supplemental Material [47], we extend the refutation of XQUATH even for 2D circuits. Concretely, XQUATH states that there is no polynomial time classical algorithm to get an estimation $q_U(0^N)$ of $p_U(0^N)$ (the probability of getting 0^N from the ideal circuit given a circuit U) up to a precision approximately 2^{-N} (see the Supplemental Material [47] for more detail), which is slightly better than randomly guessing. In the Supplemental Material [47], we prove that this precision is exactly the average XEB, $\langle \chi_U(C) \rangle_U$. Thus if

the precision 2^{-N} can be modified to $e^{-\Delta d}$ for some constant Δ (where $\Delta \sim \Delta_1$ for 1D circuit), then our algorithm, which runs in linear time, could achieve this approximation. We argue that the modification is reasonable because in order to get a chaotic circuit, $d \sim N$ for 1D and $d \sim$ $\sqrt{N} \ll N$ for 2D [18,65]. The original motivation of this conjecture was to establish a connection between the hardness of the sampling problem and the hardness of a direct simulation of quantum circuit. Since our algorithm is far from direct simulating a quantum circuit, our result implies that the precision required in XQUATH, is not accurate enough in order to capture the hardness of direct simulation; however, our result for 1D noisy circuit shows that, more accurate precision is even not reasonable to a quantum device without fault tolerance. In the Supplemental Material [47], we also show that a similar (although slightly weaker) refuting statement also holds for 2D or even more general circuit architectures.

Finally, we remark that, our algorithm is not trying to simulate noisy circuits like the one in Ref. [66]. Instead, the only objective of our algorithm is to get high XEB value, but the associated fidelity might be very low (even much lower than what a noisy circuit could have). Conceptually, our algorithm is a generalization of the one in Ref. [67] beyond shallow circuits. The present results constitute substantial improvements and extensions of this algorithm, with a thorough theoretical analysis and detailed numerical simulations.

IV. UNDERSTANDING XEB AND FIDELITY VIA CLASSICAL STATISTICAL MECHANICS

In this section, we assume the single-qubit gate is Haar random and present an analytic framework to understand the relation between the XEB and the fidelity under various conditions, including different quantum circuit architectures and the presence of noise or omitted gates. We will find that, in these settings, both the XEB and the fidelity, averaged over an ensemble of unitary circuits, can be efficiently estimated by mapping the quantum dynamics to classical statistical mechanics models, such as the diffusion-reaction model. This mapping to the diffusionreaction model was previously developed in Ref. [50] for the purpose of studying quantum information scrambling under random circuit dynamics. Here we use a similar method to study behavior of the XEB and fidelity in random circuits with various entangling gates. In the special case of 1D circuits, the effective model can be further simplified to a ferromagnetic Ising spin model in two dimensions, allowing us to obtain the scaling behavior analytically.

A. Overall methodology

We first outline how quantum dynamics can be mapped to a classical statistical mechanics model. The XEB and the fidelity can be written as

$$\chi_U + 1 = \sum_{x} \langle x | U \rho_0 U^{\dagger} | x \rangle \langle x | \mathcal{M}_U^{(a)}[\rho_0] | x \rangle 2^N, \quad (8)$$

$$F_{U} = \sum_{x,x'} \langle x | U \rho_{0} U^{\dagger} | x' \rangle \langle x' | \mathcal{M}_{U}^{(a)} [\rho_{0}] | x \rangle, \qquad (9)$$

where $\rho_0 = |0^N\rangle\langle 0^N|$ is the initial state of the system, and $\mathcal{M}_U^{(a)}[\cdot]$ is a quantum channel associated with the ideal unitary evolution (a=ideal), noisy quantum dynamics (a=noisy), or our classical algorithm with omitted gates (a=algo). For a different choice of $a=\{\text{ideal},\text{noisy},\text{algo}\}$, Eqs. (8) and (9) become the XEB and the fidelity of the corresponding case, respectively. The sum over x,x' represents the summation over all possible N-qubit configurations (bitstrings).

The key idea is to realize that both the XEB and the fidelity can be expressed as the expectation values of observables in an extended Hilbert space. More explicitly, we envision having two identical copies of the Hilbert space: one representing the ideal circuit dynamics, and the other representing the dynamics in either the ideal circuit, noisy circuit, or our algorithm [see Fig. 8(a)]. Then, we have

$$\chi_U + 1 = \text{Tr}\mathcal{B}_{XEB} \left(U \rho_0 U^{\dagger} \otimes \mathcal{M}_U^{(a)}[\rho_0] \right),$$
 (10)

$$F_U = \operatorname{Tr} \mathcal{B}_F \left(U \rho_0 U^{\dagger} \otimes \mathcal{M}_U^{(a)}[\rho_0] \right), \tag{11}$$

where $\mathcal{B}_{XEB} = 2^N \sum_x |x\rangle \langle x| \otimes |x\rangle \langle x|$ and $\mathcal{B}_F = \sum_{x,x'} |x\rangle \langle x'| \otimes |x'\rangle \langle x|$ are Hermitian observables defined in the enlarged space. In the following, we simply use \mathcal{B}_b with $b \in \{XEB, F\}$.

A convenient way to study the type of operators in Eqs. (10) and (11) is to represent them as tensor networks whose contraction results in $\chi_U + 1$ or F_U , as shown in Figs. 8(a), 8(b). In general, the contraction of these tensor network diagrams for any given U would be computationally difficult, as it is equivalent to evaluating the corresponding quantum circuit. However, we are mostly interested in the average-case behavior of a class of random quantum circuits with gates drawn from specific gate ensembles. In this case, we can perform the averaging over the gate ensemble before contracting the network. Crucially, we find that the averaging process allows us to re-express the tensor network as a summation over exponentially many simple diagrams enumerated by different configurations of classical variables s [see Fig. 8(b)].

This emergent mathematical structure—namely the summation over all possible configurations of classical variables—is similar to the path-integral formulation of a classical Markov process, or a partition function in statistical mechanics models [68]. Indeed, we will show that $\chi_U + 1$ and F_U , averaged over an ensemble of unitary gates, are *exactly* described by a diffusion-reaction model or a classical Ising spin model.

B. The emergent diffusion-reaction model

We now describe the exact mapping from random unitary circuits to the diffusion-reaction model. To derive this mapping, we will first consider the bulk of the tensor network in the absence of any noise or omitted gates, i.e., $\mathcal{M}_U^{\text{ideal}}[\rho_0] = U\rho_0 U^{\dagger}$. We will follow with the analysis of the boundaries at t=0 (initial state) and at t=d (contraction with the observable \mathcal{B}_b). Finally, we will consider how the presence of noise or omitted gates influences the system.

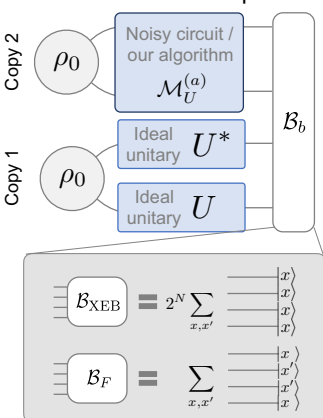
1. Bulk of the ideal circuit

The central ingredient of the mapping to statistical mechanics models is the averaging over an ensemble of unitary gates [69]. In our case, we consider a single-qubit unitary $u \in SU(2)$ averaged over the Haar ensemble (or any other ensemble that forms a unitary 2-design). As depicted in Fig. 8(b), every random unitary u appears exactly 4 times: a pair of u and u^{\dagger} for the ideal dynamics and another pair for the quantum channel $\mathcal{M}_U^{(a)}$. Since these sets of four random gates are independent, we can average them locally within the circuit using the 2-design property [69],

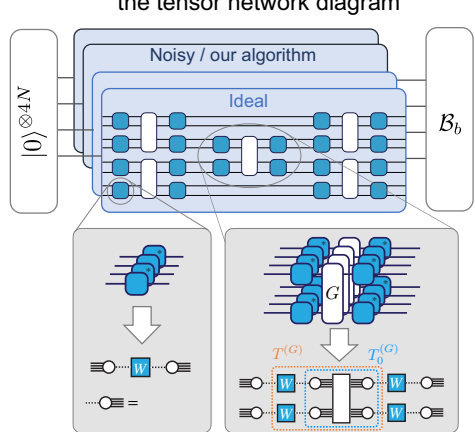
$$\mathbb{E}_{u}[u \otimes u^{*} \otimes u \otimes u^{*}] = |I\rangle\langle\langle I| + \frac{1}{3}|\Omega\rangle\rangle\langle\langle\Omega|, \quad (12)$$

where $|I\rangle\rangle$ and $|\Omega\rangle\rangle$ are mutually orthogonal operators in the duplicated Hilbert space defined as

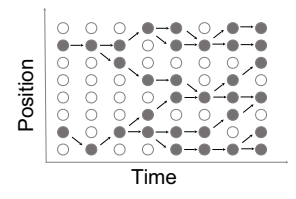
(a) Tensor-network representation in doubled Hilbert space



(b) Averaging over unitary gates in the tensor network diagram



(c) Diffusion-reaction model



(d) Ising spin model

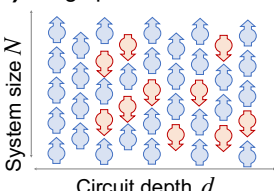


FIG. 8. Mapping quantum circuits to statistical mechanics models. (a) Both XEB and fidelity can be written as observables \mathcal{B}_b with b = XEB, F in a duplicated Hilbert space by using tensor-network representations. The duplicated Hilbert space consists of the tensor product of copy 1, representing an ideal circuit evolution, and copy 2, representing the dynamics of either noisy circuit or our algorithm with omitted gates. (b) For the tensor-network diagrams representing XEB or fidelity, each random unitary gate (blue boxes) and its complex conjugate (blue boxes with asterisks) appear twice: in copy 1 and in copy 2. One can perform averaging over an ensemble of unitary gates without explicitly evaluating the tensor-network diagram, which gives rise to a simpler tensor network diagram with new classical variables, s, associated with each averaged single-qubit unitary gate (bottom left). Entangling unitary gates G dictate the dynamics of variables s, which is encapsulated in the transfer matrices of the classical statistical mechanics model (bottom right). (c) Schematic diagram for the diffusion-reaction model. Each site can be occupied by a particle (filled) or remain unoccupied (empty). In every discrete time step, each particle may either stay on the same site, move to a neighboring site (diffusion), or duplicate itself to a neighboring site (reaction). Finally, a pair of particles located on neighboring sites may recombine into a single particle (reaction). Each of these processes has a specific probability that depends on the underlying gate ensemble. (d) Quantum circuits in 1D can be mapped to the classical Ising spin model in 2D.

$$\langle \langle a, b, c, d | I \rangle \rangle = \frac{1}{2} \delta_{ab} \delta_{cd},$$

$$\langle \langle a, b, c, d | \Omega \rangle \rangle = \frac{1}{2} \sum_{\mu = x, y, z} \sigma_{ab}^{\mu} \sigma_{cd}^{\mu},$$
(13)

with Pauli matrices σ^{μ} , and $a,b,c,d\in\{0,1\}$. We note that by using this notation, we are implicitly utilizing the channel-state duality (also known as the Choi-Jamiołkowski isomorphism [70]), where operators such as density matrices are vectorized: $\rho = \sum_{ij} \rho_{ij} |i\rangle \langle j| \rightarrow |\rho\rangle \rangle = \sum_{ij} \rho_{ij} |i\rangle |j\rangle$. Intuitively, $\langle\langle I|$ and $\langle\langle \Omega|$ represent the normalization and the total polarization correlation between the two copies, respectively; see the Supplemental Material [47] for the detailed derivation of these properties.

Notice that Eq. (12) is a sum of two projectors, up to normalization factors. Therefore, by applying Eq. (12) to every quadruple of single-qubit unitary gates, the tensornetwork diagram factorizes into smaller parts, which are enumerated by different assignments of classical variables $s \in \{I, \Omega\}$ associated with every independent single-qubit unitary gate. We interpret the classical variable s at a certain site in space time as if that site is in a vacuum state (s = I) or occupied by a particle ($s = \Omega$). In this picture, the particle configuration at a specific time step is given by

the assignment of I or Ω values to s variables within that time slice. Then, the tensor network describes how the particle configuration is advanced in every time step, which is captured by the transfer matrix \mathcal{T} .

The transfer matrix between two time steps is determined by the product of local transfer matrices $\mathcal{T} = \prod_G T^{(G)}$. In turn, a local transfer matrix $T^{(G)}$ is given by the combination of the prefactor 1/3, originating from Eq. (12), and a nontrivial contribution $T_0^{(G)}$ associated with a single two-qubit gate G, as shown in Fig. 8(b). We evaluate $T_0^{(G)}$ explicitly by contracting (four copies of) a two-qubit gate G with four vectors $|s\rangle\rangle$, where $s=I,\Omega$, arising from four single-qubit random gates before and after G [see Fig. 4(b)]:

$$T_{0;s_1s_2s_3s_4}^{(G)} = \langle \langle s_1 | \langle \langle s_2 | G \otimes G^* \otimes G \otimes G^* | s_3 \rangle \rangle | s_4 \rangle \rangle. \tag{14}$$

Explicit calculations lead to the general form of the T matrix

$$T^{(G)} = \begin{pmatrix} 1 & 0 & 0 & 0\\ 0 & 1 - D & D - R & R/\eta\\ 0 & D - R & 1 - D & R/\eta\\ 0 & R & R & 1 - 2R/\eta \end{pmatrix},$$
(15)

TABLE II. Values of the diffusion rate D and the reaction rate R for a few different entangling gates.

	CZ	Haar	fSim	fSim*
Diffusion rate D	2/3	4/5	1	1
Reaction rate R	2/3	3/5	$1/3 + \sqrt{3}/6$	2/3

written in the basis $\{II, I\Omega, \Omega I, \Omega\Omega\}$. This formula has been derived in Ref. [50] for studying quantum scrambling. In this work, we apply it to study vulnerabilities of the XEB. Here, $D \ge 0$ and $R \ge 0$ are parameters that depend on the specific choice of the entangling unitary gate G (the gate ensemble), while $\eta = 3$ for any two-qubit gate. We call D, R, and η , the diffusion rate, reaction rate, and reaction ratio, respectively, and summarize their values for a few common entangling gates in Table II.

We note that each column of T is normalized to unity, implying that the matrix indeed describes a transfer matrix for a stochastic process. For example, the entry in the second column and the fourth row specifies the probability of the two sites going from $I\Omega$ to $\Omega\Omega$ —this is an example of the "reaction" process. Other transitions are given in the following, with probabilities written on top of the arrows,

vacuum:
$$II \xrightarrow{1} II$$
stay: $I\Omega \xrightarrow{1-D} I\Omega, \Omega I \xrightarrow{1-D} \Omega I$
move: $I\Omega \xrightarrow{D-R} \Omega I,$
 $\Omega I \xrightarrow{D-R} I\Omega, \quad \Omega \Omega \xrightarrow{1-2R/\eta} \Omega \Omega$
duplication: $I\Omega, \Omega I \xrightarrow{R} \Omega \Omega$
recombination: $\Omega \Omega \xrightarrow{R/\eta} I\Omega, \Omega I.$

The third process (move) is the "diffusion" (i.e., random walk), while the last two (duplication and recombination) are reaction processes, i.e., particle creation and annihilation. Notice that a particle cannot be created from the vacuum or annihilated into the vacuum without interacting with another particle.

2. Boundary conditions at the initial state and at the final time

Next, we turn to the boundaries of our tensor network diagram. First, we contract the input state $\rho_0 \otimes \rho_0$, denoted as $|0^{\otimes 4}\rangle\rangle^{\otimes N}$, with tensors associated with all 2^N possible particle configurations. This leads to the vector $\mathbf{u}^{\otimes N}$, where

$$\mathbf{u} = \begin{pmatrix} \langle \langle I | 0^{\otimes 4} \rangle \rangle \\ \langle \langle \Omega | 0^{\otimes 4} \rangle \rangle \end{pmatrix} = \begin{pmatrix} 1/2 \\ 1/2 \end{pmatrix}, \tag{16}$$

which follows directly from Eq. (13). This vector describes the initial distribution of particles: every site is occupied by a particle or remains empty with probabilities 1/2.

Similarly, at the final layer, we contract the \mathcal{B}_b observables with tensors associated with all 2^N possible particle configurations, leading to dual vectors $\mathbf{v}_{\text{XEB}}^{\top \otimes N}$ and $\mathbf{v}_F^{\top \otimes N}$ for the XEB and the fidelity, respectively, where

$$\mathbf{v}_{\mathrm{XEB}}^{\top} = \left(\langle \langle I | \beta_{\mathrm{XEB}} \rangle \rangle \quad \frac{\langle \langle \Omega | \beta_{\mathrm{XEB}} \rangle \rangle}{3} \right) = \begin{pmatrix} 2 & 2/3 \end{pmatrix}, \\ \mathbf{v}_{F}^{\top} = \left(\langle \langle I | \beta_{F} \rangle \rangle \quad \frac{\langle \langle \Omega | \beta_{F} \rangle \rangle}{3} \right) = \begin{pmatrix} 1 & 1 \end{pmatrix},$$
(17)

and

$$|\beta_{\text{XEB}}\rangle\rangle = 2\sum_{i\in\{0,1\}}|i\rangle|i\rangle|i\rangle|i\rangle,$$
 (18)

$$|\beta_F\rangle\rangle = \sum_{i,i'\in\{0,1\}} |i\rangle |i'\rangle |i'\rangle |i\rangle,$$
 (19)

are the single-site versions of \mathcal{B}_b , i.e., $\mathcal{B}_b = \beta_b^{\otimes N}$. We find that \mathbf{v}_{XEB} is distinguished from \mathbf{v}_F by unequal weights between I and Ω (by a factor of 1/3) aside from the global normalization factor 2. This allows an intuitive explanation: as previously mentioned, $\langle\langle\Omega|$ represents total polarization correlation between two copies of quantum states, but XEB depends only on correlations measured in the computational basis constituting 1/3 of the total on average.

Combining the results from bulk transfer matrices, and initial and final boundary conditions, we obtain the expression for the ensemble-averaged XEB and fidelity:

$$\chi_{\text{av}} + 1 \equiv \mathbb{E}_{u}[\chi_{U}] + 1 = \mathbf{v}_{\text{XEB}}^{\top \otimes N} \left(\prod_{j=1}^{d} \mathcal{T}_{j} \right) \mathbf{u}^{\otimes N}$$
(20)

$$F_{\text{av}} \equiv \mathbb{E}_{u}[F_{U}] = \mathbf{v}_{F}^{\top \otimes N} \left(\prod_{j=1}^{d} \mathcal{T}_{j} \right) \mathbf{u}^{\otimes N}, \tag{21}$$

where \mathcal{T}_j is the transfer matrix for N particles at time step j.

3. XEB and fidelity as statistics of a particle distribution

Our results in Eqs. (20) and (21) allow for an intuitive understanding of the XEB and the fidelity in terms of particle distributions in the diffusion-reaction model. We note that these two quantities differ only by the boundary condition at the final time t = d, as defined in Eqs. (18) and (19). Hence, both the XEB and the fidelity are fully determined by the probability distribution of particle configurations, \mathbf{p} , obtained by evolving the initial uniform distribution $\mathbf{u}^{\otimes N}$

for *d* time steps:

$$\mathbf{p} \equiv \mathcal{T}_d \cdots \mathcal{T}_2 \mathcal{T}_1 \mathbf{u}^{\otimes N}. \tag{22}$$

From this distribution, the XEB and the fidelity can be evaluated by simply contracting either $\mathbf{v}_{\mathrm{XEB}}^{\top\otimes N}$ or $\mathbf{v}_F^{\top\otimes N}$, which corresponds to computing certain statistics of the particle distribution. For instance, all entries in $\mathbf{v}_F^{\top\otimes N}$ are unities, implying that $\mathbf{v}_F^{\top\otimes N}\mathbf{p}$ is equal to the summation over all probabilities:

$$F_{\text{av}} = \mathbf{v}_F^{\top \otimes N} \mathbf{p} = \mathbb{E}_{\mathbf{p}}[1], \tag{23}$$

where $\mathbb{E}_{\mathbf{p}}[\cdot]$ denotes the averaging over the distribution \mathbf{p} . In the absence of any noise or omitted gates, the transfer matrix in Eq. (15) preserves the total probability, leading to $F_{av} = \mathbb{E}_{\mathbf{p}}[1] = 1$. This result is trivially expected in the quantum circuit picture—in the absence of any noise or omitted gates, the fidelity must always be unity. We will soon see how this picture is modified when we introduce noise or omit gates.

Similarly, the average XEB is

$$\chi_{av} + 1 = \mathbf{v}_{XEB}^{T \otimes N} \mathbf{p} = 2^N \mathbb{E}_{\mathbf{p}} \left\lceil \frac{1}{3^{\#\Omega \text{ in the last layer}}} \right\rceil,$$

where $\#\Omega$ denotes the total number of particles.

4. Effects of noise or omitted gates

When unitary dynamics is interspersed by noise channels $(\mathcal{M}_U^{\text{(noisy)}})$ or when some of the gates are omitted in our classical algorithms $(\mathcal{M}_U^{\text{(algo)}})$, only the bulk part of the tensor network changes, leading to a modified transfer matrix. For a noisy circuit, the new transfer matrix is

$$T_{\epsilon}^{(G)} = (I_{\epsilon} \otimes I_{\epsilon}) T^{(G)} \quad \text{with } I_{\epsilon} = \begin{pmatrix} 1 & 0 \\ 0 & 1 - c\epsilon \end{pmatrix}, \quad (24)$$

where c is a constant depending on the type of noise. For example, c=4/3 for the depolarizing noise $\mathcal{N}_{\epsilon}(\rho)=(1-\epsilon)\rho+\epsilon/3\sum_{\mu}\sigma^{\mu}\rho\sigma^{\mu}$, and c=2/3 for the amplitude damping noise.

Unlike the transfer matrix in the ideal case, the noisy-circuit transfer matrix in Eq. (24) no longer describes a stochastic process. That is, the sum of each column in $T_{\epsilon}^{(G)}$ is less than unity, implying that the probability is not conserved. Thus, the effect of noise gives rise to the "loss of probability" in our diffusion-reaction model. In general, this leads to an unnormalized final distribution \mathbf{p} and reduced average fidelity $F_{\rm av} < 1$. Crucially, the loss of probability occurs only when a particle (Ω) is present at a given space-time point. The diagonal entries in I_{ϵ} imply that the probability associated with a given particle configuration will be damped by a factor $(1 - c\epsilon)^{\#\Omega}$ at every

time step. Therefore, we expect an interesting interplay between the diffusion-reaction dynamics of particles and the probability loss.

For our classical algorithm, it is the omission of gates that modifies the transfer matrix. In this case, only local transfer matrices associated with an omitted gate are affected

$$T^{(G)} \to (P_I \otimes P_I) \cdot T^{(G)} = P_I \otimes P_I \quad \text{with } P_I = \begin{pmatrix} 1 & 0 \\ 0 & 0 \end{pmatrix}.$$
(25)

Similarly to the noisy circuit case, the omission of gates also causes the loss of probabilities; thus, the fidelity becomes smaller than 1. More specifically, Eq. (25) implies that, at any given time, the probability weights associated with particle configurations containing at least one particle at the site of omitted gates must vanish; such configurations do not contribute to the average XEB or fidelity. Thus, the only nonvanishing contributions arise from diffusion-reaction processes in which not a single particle ever appears at the sites of omitted gates throughout the entire dynamics. The average fidelity will then be the total probability of such diffusion-reaction processes, and the average XEB is determined by the resultant unnormalized distribution **p**.

We remark that the deterministic loss of probability at the positions of omitted gates leads to the factorization of the transfer matrix in Eq. (25) (as a product of two projectors). Due to this factorization, **p** for the whole system also factorizes into independent probability vectors for two isolated subsystems. This feature allows the numerical calculation of the average XEB for system sizes up to the quantum advantage regime (60 qubits, depth 24).

C. Dynamics of the XEB and fidelity

Having introduced the mapping of random unitary circuits to the diffusion-reaction model in the previous section, we now leverage this formalism to understand the quantitative behavior of the XEB and the fidelity under various conditions. In particular, we explain the key concepts used to obtain results presented in Sec. III.

1. Ideal circuit

In the absence of noise and omitted gates, the fidelity remains equal to unity trivially, due to the conservation of the total probability. It is nontrivial, however, to see how the average XEB approaches unity in the limit of deep quantum circuits [5], which we now explain in terms of diffusion-reaction dynamics. Both the XEB and the fidelity, at late times (large depths), are determined by the output vector \mathbf{p} . For the transfer matrix in Eq. (15), this distribution converges to a fixed point in the large-depth limit. In the current case, there are two fixed points for local transfer matrices, $\mathbf{u}_1 = (1/4, 3/4)$ and $\mathbf{u}_2 = (1, 0)$. The former

represents a nontrivial steady-state solution in which the total normalization, and three different types of correlations (along x, y, and z directions) are equally distributed, while the latter represents a trivial solution where two copies are both in completely mixed states; hence, no correlation is generated during dynamics. It can be shown that the global stationary distribution is given as a mixture of $\mathbf{u}_1^{\otimes N}$ and $\mathbf{u}_2^{\otimes N}$, whose ratio is determined by the initial condition $\mathbf{u}_2^{\otimes N}$:

$$\lim_{d \to \infty} \mathbf{p} = (1 - 2^{-N})\mathbf{u}_1^{\otimes N} + 2^{-N}\mathbf{u}_2^{\otimes N} + O(4^{-N}).$$
 (26)

The dominant contribution originates from the nontrivial equilibrium configuration \mathbf{u}_1 , whereas the \mathbf{u}_2 term constitutes a small correction.

The nontrivial term describes the homogeneous distribution of particles with the density 3/4, as shown in Fig. 9(a), contributing to the XEB

$$\mathbf{v}_{\text{XEB}}^{\top}\mathbf{u}_1 = 2\left(\frac{1}{4} \times 1 + \frac{3}{4} \times \frac{1}{3}\right) = 1.$$

The trivial term gives $\mathbf{v}_{\text{XEB}}^{\top}\mathbf{u}_2 = 2$ per site. Combined together with appropriate coefficients, we obtain the average XEB $\chi_{\text{av}} = (1-2^{-N}) \approx 1$ as expected. We note that the net contribution from the trivial solution (\mathbf{u}_2 term) is always +1, which exactly cancels the constant term -1 in the definition of the XEB.

2. Noisy circuit

If noise is introduced to the system, the total probability is no longer conserved, and $\mathbf{u}_1^{\otimes N}$ does not form a stationary solution. However, we can still predict the behavior of the average XEB and fidelity using our model. We distinguish two regimes: (a) the weak-noise limit where the total probability loss rate $N\epsilon$ is much smaller than the inverse equilibration time $\tau_{\rm eq}^{-1}$ of the particle distribution, $N\epsilon \ll \tau_{\rm eq}^{-1}$, and (b) strong-noise limit $N\epsilon \gg \tau_{\rm eq}^{-1}$. In terms of quantum circuit dynamics, these conditions correspond to the comparison of the total error rate to the scrambling time.

In the limit of weak noise, the steady-state configuration must stay close to that of the equilibrium solution, because the system relaxes quickly before any substantial probability loss occurs. Thus, the output probability vector at the final time is not severely affected by the probability loss during preceding times, other than a global rescaling factor. This leads to the (un-normalized) equilibrium state $\widetilde{\mathbf{p}} = \widetilde{\mathbf{u}}_1^{\otimes N}$, where

$$\widetilde{\mathbf{u}}_1 \approx \alpha \begin{pmatrix} 1/4 \\ 3/4\beta \end{pmatrix}$$
. (27)

Here α is the rescaling factor that accounts for the probability loss (per site) during the diffusion-reaction dynamics,

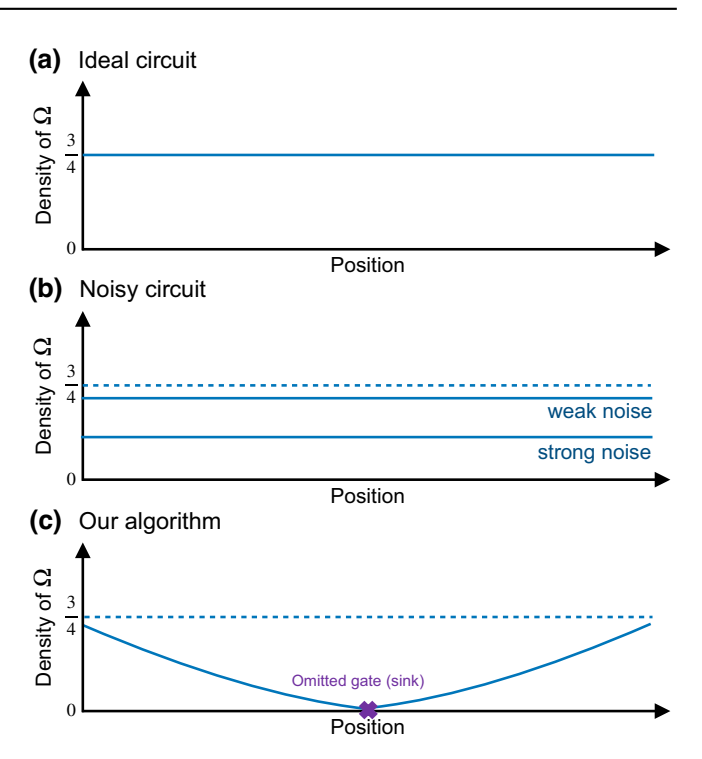


FIG. 9. Sketch of the particle population distribution at the last layer. The vertical axis is the density of particles (Ω) at the final layer normalized by the total probability, and the horizontal axis is the position of sites. (a) Ideal circuits. (b) Noisy circuits. The density is decreased relatively to the ideal case. The discrepancy becomes larger for larger noise rates. (c) Our algorithm. Close to the position of an omitted gate, or a "sink" (purple cross), the density of particles is suppressed.

and it generally decreases exponentially with depth. The parameter β quantifies the deviation of $\widetilde{\mathbf{u}}_1$ from its equilibrium shape, and generally $\beta \approx 1$ in the weak-noise limit. The precise value of β depends on the strength of noise and the equilibration time. As long as $\beta \approx 1$, $\widetilde{\mathbf{p}}$ is a simple rescaling of the ideal-circuit distribution, and XEB approximates the fidelity well; both quantities are suppressed by the factor of α^N .

In the limit of relatively strong noise (slow equilibration), the particle configuration cannot relax to its equilibrium before it is significantly affected by the probability loss. In this limit, the deviation of $\tilde{\mathbf{u}}_1$ from the equilibrium becomes significant, and $\beta < 1$ decreases with the increasing strength of noise. This is because, generically, the probability loss associated with Ω particles during dynamics results in a reduced density of particles at the last layer [see Fig. 9(b)]. The reduced density of particles implies that the XEB is larger than the fidelity because the boundary vector \mathbf{v}_{XEB} has a higher weight for the vacuum than for the particle state, whereas \mathbf{v}_F has the same weight for both states. Hence, the larger the noise rate, the greater the deviation of the XEB from the fidelity. Equation (27) no longer holds for greater noise strengths [71].

3. Spoofing algorithm

Our algorithm is designed to leverage the discrepancy between the XEB and the fidelity. In contrast to homogeneous errors spread over the bulk of the circuit, the errors in our algorithm are highly inhomogeneous and localized—they appear only at specific positions where we omit gates. This inhomogeneity leads to a particle distribution that is far from its equilibrium counterpart. More specifically, the position of an omitted gate behaves like a "sink" of probabilities—any configurations containing particles at sink sites, at any time, will acquire vanishing contribution to $\widetilde{\mathbf{p}}$. Therefore, in any nonvanishing contribution to $\widetilde{\mathbf{p}}$, the relative density of particles with respect to the density of vacuum states is substantially lowered near the sink [see Fig. 9(c)]. This large imbalance (relative to the equilibrium) leads to the large XEB-to-fidelity ratio. Thus, given the same value of fidelity, which is controlled by the total number of omitted gates, one can achieve high XEB values because vacuum state I has a larger weight in the XEB than in the fidelity.

The nonequilibrium, spatially inhomogeneous dynamics of particles also leads to a distinct scaling behavior. In our algorithm, the average XEB value increases with the system size N, when the number of omitted gates is fixed. This can be intuitively explained: the more space for particles to diffuse to, the less likely it is for them to hit sink sites, leading to an effectively smaller particle loss rate and reduced imbalance in the particle density, relative to the equilibrium.

Here, we make two remarks. First, while our analysis remained qualitative and focused on two extreme cases of error models, i.e., one with completely homogeneous noise and another fully localized errors, we emphasize that our intuitive understanding can be straightforwardly generalized to arbitrary circuit geometry with arbitrary inhomogeneous error models in both space and time. In such cases, one can directly estimate the distribution $\tilde{\mathbf{p}}$ by using conventional approaches, such as Monte Carlo methods. Second, we comment that, intuitively, larger diffusion and reaction rates imply a shorter time required to reach the equilibrium distribution. In other words, given a circuit architecture, the XEB will be on average a better proxy for the fidelity in circuits consisting of faster scrambling (entangling) gates, with larger R and D.

4. Numerical demonstration

To corroborate our predictions based on the diffusion-reaction model, we present the results of our numerical simulations. First, we confirm that the XEB overestimates the fidelity, and that the discrepancy is larger for higher noise rates, as shown in Fig. 10. We find that the fSim ensemble has the smallest XEB-to-fidelity ratio. The reason for this is clear from the diffusion-reaction model: among the three gates we considered, their reaction rates

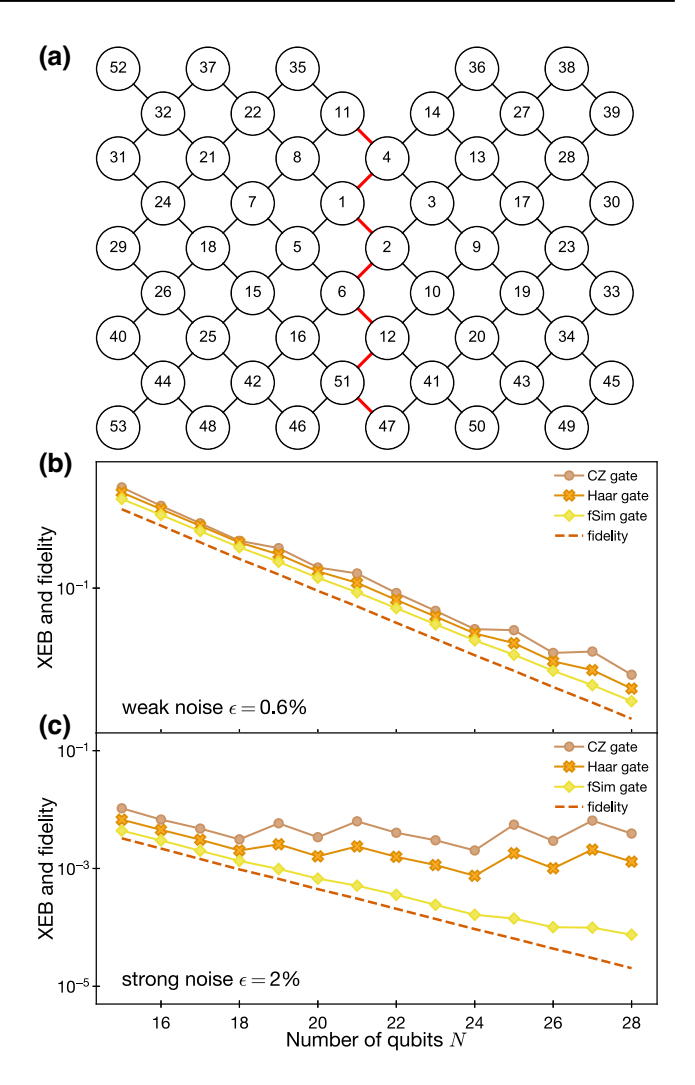


FIG. 10. XEB versus fidelity in noisy circuits. The XEB always overestimates the fidelity, but the deviation depends on the gate ensemble and the strength of noise. (a) For this calculation, we use the original qubit ordering from Fig. S25 in Ref. [5] (see also Fig. 5). (b) Weak-noise regime ($\epsilon=0.6\%$). The XEB approximates the fidelity well, and the fidelity values for all gate ensembles are almost the same. (c) Strong-noise regime ($\epsilon=2\%$). The quality of the XEB-to-fidelity approximation strongly depends on the choice of the gate ensemble. Among the three ensembles considered here, the fSim ensemble gives the best result.

R are similar (between 0.6 and 0.67), but the fSim gate has the largest possible diffusion rate D=1, as shown in Table II.

We use this intuition to devise an even better gate, which we call the fSim*. By fixing D = 1, we find that the fSim* gate has a larger R = 2/3. Moreover, these values of R and D are now optimal, which we prove in the Supplemental Material [47]. Thus, fSim* has the smallest possible discrepancy between the XEB and the fidelity. We compare it to the fSim gate in the inset of Fig. 3(b).

Next, we verify that the average XEB value of our algorithm for a specific circuit architecture (the Sycamore

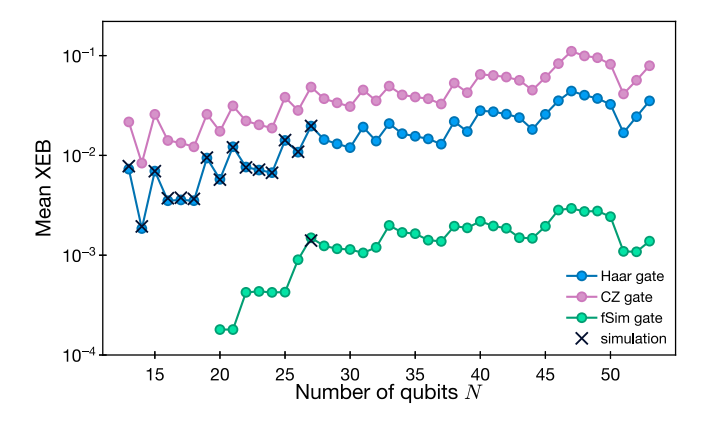


FIG. 11. Mean XEB value obtained by our algorithm as a function of the system size N, using the ordering in Fig. 10(a) and the d=14 circuit architecture from Ref. [5]. The average XEB values are calculated using the diffusion-reaction model for three different gate ensembles: Haar (blue), CZ (purple), and fSim (green). When compared with the results of the direct simulation of quantum circuits (crosses), both methods agree very well.

chip) can be very accurately predicted by our diffusion-reaction model. These results are shown in Fig. 11. We find that our diffusion-reaction model can predict even the fine details of the scaling with the system size N. For example, in Fig. 11, the rise and fall in the value of XEB is caused by the lattice structure [see Fig. 10(a)] and its effect on the diffusion process.

D. Ising model for 1D Haar ensembles

The diffusion-reaction model is useful for analyzing our system qualitatively and numerically, for general circuit architectures and two-qubit gate sets. However, for a certain class of systems, such as 1D circuits with Haar two-qubit gates, one can further simplify the classical statistical physics model to the 2D Ising model. This can be understood as a special case of the diffusion-reaction model, related to it mathematically through a basis transformation. This mapping has been studied previously in Refs. [51–57,72]. The Ising model allows us to obtain more quantitative results. We find that the behavior of the XEB is related to symmetry, symmetry breaking, and magnetization.

The basis change from the diffusion-reaction model to the Ising model is

$$|\uparrow\rangle\rangle = 2|I\rangle\rangle,$$

 $|\downarrow\rangle\rangle = |I\rangle\rangle + |\Omega\rangle\rangle,$

such that

$$\langle \langle a, b, c, d | \uparrow \rangle \rangle = \delta_{ab} \delta_{cd},$$
$$\langle \langle a, b, c, d | \downarrow \rangle \rangle = \delta_{ad} \delta_{bc},$$

where the second equation indicates that $|\downarrow\rangle\rangle$ corresponds to a swap between indices a and c (or b and d). This new basis reflects the symmetry in $u \otimes u^* \otimes u \otimes u^*$ between the two copies: the state is invariant if we exchange the positions of the two us or u^* s (labeled by a, c and b, d, respectively).

We regard \uparrow and \downarrow as the up and down spins, and the path integral of the diffusion-reaction dynamics is mapped to the partition function of the spin model [see Fig. 8(d)]. In the absence of noise or omitted gates, the partition function has a global \mathbb{Z}_2 Ising symmetry, such that $|\uparrow\rangle\rangle \leftrightarrow |\downarrow\rangle\rangle$ applied to all spins does not change the partition function.

After the basis change, XEB + 1 corresponds to the partition function of the \mathbb{Z}_2 -symmetric Ising spin model with identical boundary conditions at both the initial and final times. In the special case of Haar entangling gates, this model is the ordinary Ising model with two-body interactions, which are detailed in the Supplemental Material [47] and Refs. [51–57,72].

This mapping allows us to write the XEB for the ideal circuit in the following form:

$$\chi_{\text{ideal}} + 1 = Z = \langle \langle \psi | \mathcal{T}_{\text{Ising}}^{(d-1)/2} | \psi \rangle \rangle,$$
 (28)

where $|\psi\rangle\rangle$ and $\langle\langle\psi|$ are the boundary conditions, and $\mathcal{T}_{\text{Ising}}$ is the transfer matrix of the Ising model along the horizontal direction in Fig. 8(d); it is semidefinite positive and can be computed from $T_0^{(\text{Haar})}$ and Eq. (12). We defer the details of this calculation to the Supplemental Material [47]. Here, we only need to know that this Ising model is in the ferromagnetic phase. Thus, the largest eigenvalue of $\mathcal{T}_{\text{Ising}}$ is doubly degenerate, which gives Z=2 and so XEB = 1 in the large-d limit.

Once noise or gate defects are introduced, the Ising symmetry is violated. In the case of noisy circuits, the symmetry is violated everywhere, with each local interaction modified by the presence of effective magnetic fields with strength ϵ . Then, there will be a spectral gap $\Delta_{N,\epsilon} = \lambda_1 - \lambda_2$ in the modified $\mathcal{T}_{\text{Ising}}$, which we evaluate exactly. Figure 12(a) shows the gap as a function of the system size for various error rates. We show that in this case

$$\chi_{\text{noisy}} = O\left(e^{-\Delta_{N,\epsilon}d}\right).$$
(29)

If the violation is small enough ($N\epsilon \ll 1$), the spectral gap is $\Delta_{N,\epsilon} \propto N\epsilon$ because the total magnetic field is only a small perturbation from the ideal (symmetric) case. However, if we consider the asymptotic behavior of noisy circuits, ϵ is assumed constant, but N could be very large. In this limit, the gap will saturate to a fixed value $\Delta_{\infty,\epsilon}$, as shown in Fig. 12(a). This corresponds to the thermodynamic limit in terms of statistical physics (taking $N \to \infty$ first then $\epsilon \to 0$). In this case, even if ϵ tends to 0, as long as $N\epsilon$ is still large, there is a finite gap in $\mathcal{T}_{\text{Ising}}$. This corresponds to the phenomena of spontaneous magnetization:

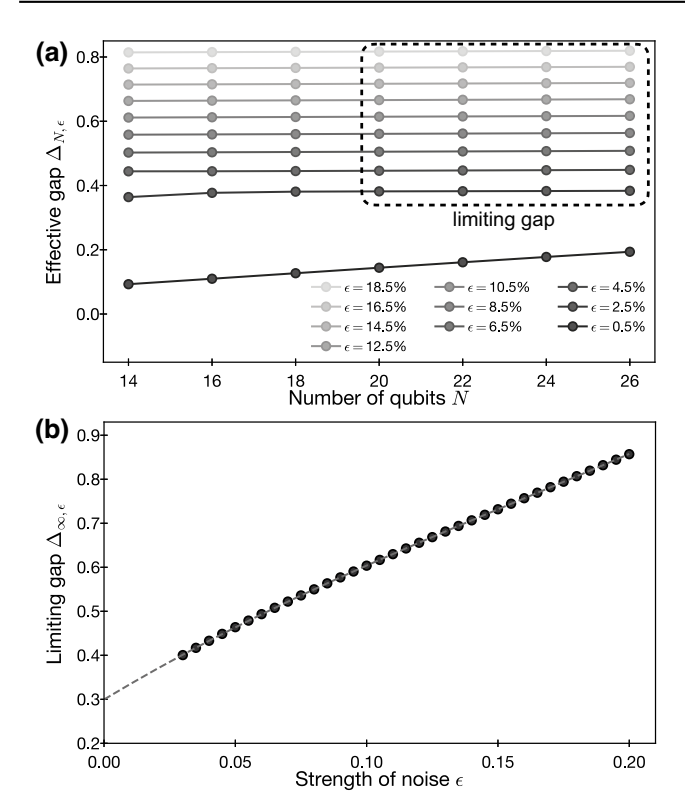


FIG. 12. Effective gaps of 1D noisy circuits. (a) For any noise strength ϵ , the gap $\Delta_{N,\epsilon}$ saturates, for sufficiently large N, at the *limiting-gap* value $\Delta_{\infty,\epsilon}$. (b) The limiting gap as a function of the noise strength. Polynomial extrapolation indicates the $\epsilon \to 0$ limit of the gap to be approximately equal to 0.03. We define this limiting value as $\Delta_3 := \lim_{\epsilon \to 0} \Delta_{\infty,\epsilon}$; in Fig. 6, it is represented by the orange, dotted horizontal line. The subsystem considered here has only one boundary with omitted gates as the total system has open boundary condition.

even if the magnetic field fades away, most of the spins still point in the same direction leading to a nonvanishing decay rate, which is the indicator of the symmetry breaking. We numerically extrapolate the limiting gap to the vanishing noise rate ϵ and get

$$\Delta_3 = \lim_{\epsilon \to 0} \Delta_{\infty,\epsilon} = \lim_{\epsilon \to 0} \lim_{N \to +\infty} \Delta_{N,\epsilon} \approx 0.3, \quad (30)$$

as shown in Fig. 12(b). This corresponds to the orange dashed line in Fig. 6.

For our algorithm, the omitted gates are mapped to a tensor product of projectors, as shown in Eq. (25), so the partition function will also be separated into the product of partition functions of isolated subsystems

$$\chi_{\text{algo}} = Z - 1 = \prod_{i=1}^{\lceil N/I \rceil} Z_l^{(i)} - 1$$
(31)

$$\approx \prod_{i=1}^{\lceil N/I \rceil} (e^{-\Delta_I^{(i)} d} + 1) - 1 \tag{32}$$

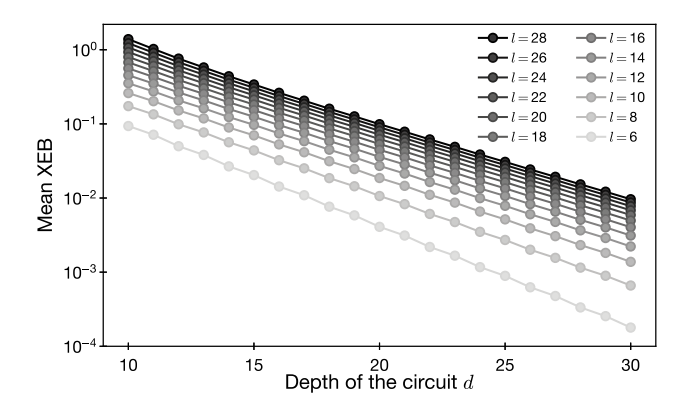


FIG. 13. Exponential decay of the average XEB value with increasing circuit depth d for our algorithm. Through linear interpolation (on the semilog plot), we compute the slope of the lines at each subsystem size l and extract the spectral gap Δ_1 . The dependence of Δ_1 on l is shown in Fig. 6 (blue solid curve).

$$\approx \sum_{i=1}^{\lceil N/l \rceil} e^{-\Delta_l^{(i)} d} \sim \frac{N}{l} e^{-\Delta_l d}, \tag{33}$$

where $\Delta_l^{(i)}$ is the gap of the *i*th subsystem, and Δ_l is the typical gap among these subsystems, assuming they have similar sizes. Equation (33) shows that the XEB increases with the system size if the subsystem size l is fixed. The decay rate is mainly determined by the subsystem with $\Delta_1 = \min_i \Delta_I^{(i)}$. For each subsystem, the omitted gates correspond to strong magnetic fields at the bottom (or top) boundary, which have been previously identified as "sinks" in our diffusion-reaction model. These fields violate the \mathbb{Z}_2 symmetry, which causes the gap to open. The gap decreases if the subsystem size *l* increases; see the discussion in the previous subsection and the Supplemental Material [47]. We numerically compute the gap for different circuit parameters and present the results in Fig. 13. We find that when $l \ge 15$, Δ_1 approaches to a constant $\Delta_1 \approx 0.25$. Crucially, we see that $\Delta_1 < \Delta_3$; this means that our algorithm generates a higher XEB value, in the large-depth limit, than noisy 1D circuits—even with arbitrarily weak noise.

1. A remark

In the above discussion, we ignored the factor in front of the exponential decay with depth. In the case of our algorithm, it is a constant (which could depend on the subsystem size l) for each subsystem because the subsystem can not distinguish how large of the total system it belongs to. Thus the factor in the total XEB grows linearly with the system size N. In the case of noisy circuit, the factor is possible to grow at most poly(N) because $d = O(\log N)$ is enough to guarantee the XEB of noisy circuit is less than 1. This is due to that the XEB of noisy circuit should be smaller than ideal circuit, XEB of ideal

circuit is exactly the anticoncentration constant and anticoncentration depth is the order of $\log N$ [67,72]. If the factor grows faster than any polynomial, $d = O(\log N)$ would not be enough to converge to 1. Since the decay rate of XEB in our algorithm is smaller than that of noisy circuit, $d = \Omega(\log N)$ makes former XEB larger.

We note that many of the qualitative behaviors discussed in this section also hold in general architectures and two-qubit gate set. For example, Eq. (33) shows that the XEB obtained by our algorithm behaves more like an additive quantity, i.e., the total XEB approximately equals the sum of XEB values for each subsystems, if they are decoupled (in our algorithm) or only weakly coupled (in noisy circuits). In contrast, fidelity exhibits multiplicative behavior, i.e., every error contributes to reducing the fidelity of the total system exponentially.

V. CONCLUSION AND OUTLOOK

In this work, we introduced a novel framework to analyze the behavior of XEB and fidelity under random quantum circuit dynamics in arbitrary architectures. We showed that the XEB generally overestimates the fidelity, and presented an intuitive explanation for this phenomenon and more quantitative analysis using a mapping of quantum dynamics to a classical diffusion-reaction model. Furthermore, leveraging our new framework, we designed a simple and efficient classical algorithm, which achieves XEB values comparable to, or even higher than, noisy circuit dynamics under various conditions. We numerically demonstrated the excellent performance of our algorithm using a relatively small amount of computational resources (time and memory), and showed that it achieves XEB values within around one order of magnitude to those obtained in experiments and by the state-of-the-art algorithms running on devices with much more computational power [39–43]. Our results demonstrate the shortcomings of the XEB for estimating the circuit fidelity and certifying quantum advantage, unless further assumptions are made. For example, our qualitative analysis in Sec. IA and quantitative results in Sec. IV indicate that, for the XEB to approximate the fidelity well, the assumption of spatially homogeneous and temporally independent weak noise is crucial. The violation of any of these conditions (as in the case of our algorithm) may lead to a substantial discrepancy between the XEB and the fidelity.

A. Overcoming the vulnerabilities of linear XEB

Our results can be used as a guideline for designing the next generation of experiments with more robust ways to certify quantum computational advantage. Here we describe a few simple methods to circumvent the shortcomings of the XEB arising from its vulnerabilities described in Sec. I A. First, we point out that the systemsize scaling of the linear XEB in our algorithm, associated

with the additive nature in Eq. (3), can be easily resolved by using a different, nonlinear benchmark such as the logarithm version of the XEB [5]. This change, however, does not address the remaining two vulnerabilities, namely (i) the deviation of the XEB from the fidelity or from the probability of having no error in the circuit, and (ii) the amplification of correlations via postprocessing in classical algorithms.

In order to address (i), one can implement quantum circuits that are scrambling faster by choosing more optimized gate sets such as the fSim* entangling gates and Google's discrete single-qubit gate set. Additionally, one could design a better circuit architecture with larger depth and more connectivity, in addition to improving the fidelity of individual gate operation. Such quantum circuits make our spoofing algorithm less effective, as partitioning the circuit into subsystems with a small number of omitted gates becomes difficult.

The amplification vulnerability arises because the previously used benchmarks are designed to quantify the correlation between bitstring probability distributions, and they are sensitive to bitstrings occurring with high probabilities. This aspect can be alleviated by using a different figure of merit. In quantum information theory, the total variation distance (TVD) is used frequently [2,11,12,16] and it seems immune to straightforward amplification methods. Unfortunately, TVD is practically intractable to estimate and hence cannot directly serve as a new benchmark [45] (see also Ref. [73] for more systematic discussion). One can argue that TVD can be instead lower bounded by the fidelity, which one can estimate using the XEB under suitable conditions. However, this approach may not be practical either because a meaningful lower bound for the TVD is obtained only for a very high value of fidelity (with the order of an inverse polynomial in the system size), which is difficult to achieve in near-term quantum devices without quantum error correction.

B. Outlook

Our work opens up a number of other new future directions. Besides the above discussion on the vulnerabilities in the adversarial settings, it is also interesting to study whether XEB can be used to certify a broader class of near-term quantum devices in real-world experiments in benign settings [35]. Assuming random circuit dynamics with homogeneous and independent error models, our analysis presents a systematic way to identify the regime where the XEB, fidelity, and the probability of no error all agree with one another. More specifically, we showed in Sec. II C within the Supplemental Material [47] that the XEB approximates the fidelity well when $N\epsilon f(c) \ll 1$, where ϵ is the local error rate and f(c) is a constant of order unity that measures a particular type of "scrambling" time for a given entangling gate. Strongly entangling gates, such

as the fSim (or the more optimal fSim*) with the discrete gate set introduced by Google [5], are an ideal choice for minimizing f(c). In the experiments performed in Refs. [5–7], $N \approx 50 \sim 60$. Assuming $f(c) \approx 1 \sim 5$, a noise rate of $\epsilon \approx 0.4\% - 2\%$ is sufficiently weak for the $N\epsilon f(c) \ll$ 1 condition to be met. The error rates in the experiments [5–7] belong to this regime. The mapping from quantum dynamics to the diffusion-reaction model [50], combined with numerical algorithms such as Monte Carlo and tensor networks [7,38–40,42,43,63], provides a quantitative method to estimate the precise value of ϵ required. Even though these error rates are weak enough, the independence and the homogeneity of noise (either in space or in time) have not been unconditionally demonstrated in the aforementioned experiments. The latter appears to be necessary in order to ensure a good agreement between the XEB and the fidelity. Alternatively, it would be interesting to explore if one could either relax the requisite conditions, or develop a more generalized relation between the XEB and the fidelity, e.g., in the presence of correlated and/or strong noise.

The mapping from quantum dynamics to classical statistical models [50] can be regarded as a de-quantization procedure of quantum circuits by randomization and averaging over an ensemble, which is similar in spirit to randomized benchmarking [74–81]. The resulting statistical model is much easier to analyze analytically and numerically. In particular, it benefits from the intuitive understanding associated with classical models, larger number of available computational tools, and connections well-studied machine-learning models, as probabilistic graphical models [82,83]. Moreover, this emergent classical model can be generalized to describe other XEB-like quantities, which are potentially useful for studying various aspects of quantum circuits. For example, by replacing ideal circuits with different quantum channels (as mentioned in the Supplemental Material [47]), the XEB can potentially detect dominant types of noise. These ideas could be explored further to design new protocols for learning and quantifying complex quantum systems. This mapping has also the potential to study other properties of random circuits, e.g., proofs of anticoncentration [67,72], convergence to the uniform distribution under Pauli noise per gate [84], and designing better simulation algorithms [66].

Our work provides strong motivation for designing new figures of merit to certify quantum advantage, which remains as an important open problem. It would be interesting to explore other efficiently measurable benchmarks that could certify the correctness of random circuit sampling. More broadly, the study of the sample complexity of certifying random circuit sampling is warranted [85]. We also notice alternative approaches to demonstrating quantum advantage. In particular, several interactive protocols have been designed recently [86–89], where

quantum features can be certified based on cryptographic and computational complexity assumptions.

ACKNOWLEDGMENTS

We would like to thank Scott Aaronson, Ehud Altman, Yimu Bao, Edward Farhi, Jin-Guo Liu, and Pan Zhang for their insightful discussions. We would like to express our special thanks to Igor Aleiner, Sergio Boixo, Sergei Isakov, Hartmut Neven, Kostyantyn Kechedzhi, and Vadim Smelyanskiy for their comments and discussions, in particular pointing out that the single-qubit gate ensemble used in recent experiments leads to near optimal performance for XEB to approximate fidelity and sharing their independent analysis of XEB based on mapping to a classical statistical mechanics model. Also, we acknowledge Jin-Guo Liu for their technical assistance regarding the use of Julia numerical package Yao and OMEinsum. This work is supported by NSF, CUA, ARO, ARO MURI, DARPA ONISQ program. X.G. is supported from Quantum Science of the Harvard-MPQ Center for Quantum Optics, the Templeton Religion Trust grant TRT 0159, and by the Army Research Office under Grant and MURI Grant . B.B. and C.C. is supported by NSF Award No. CCF 1565264, DARPA Grant No. W911NF2010021, and a Simons Investigator Fellowship. S.C. acknowledges support from the Miller Institute for Basic Research in Science.

APPENDIX A: SUMMARY OF OUR RESULTS

In this section, we list down the results of this paper for reader's reference.

Rigorous result 1: the average XEB is additive and the average fidelity is multiplicative between our algorithm and distribution from ideal circuit. The assumption is that the average is over unitary 1-design random gates.

See Sec. I A of the main text for the first place where the result is mentioned. See also Sec. I D within the Supplemental Material [47] for the proof. The concept of *t*-design is discussed in more detail in Sec. II A in the Supplemental Material [47].

Rigorous result 2: our algorithm achieves XEB value $2^{-O(d)}$ in linear time of system size and hence refutes the theoretical guarantee of XEB-based quantum computational advantage, i.e., XQUATH, in sublinear depth. The assumption is that the single-qubit gate ensemble is unitary 2-design. No assumption on two-qubit gate and circuit architecture.

See Sec. III D of the main text for the first place where the result is mentioned. See also Sec. VI in the Supplemental Material [47] for the proof.

Claim: for 1D circuits with Haar random two-qubit gate, the XEB of our algorithm is greater than noisy circuit with arbitrarily small constant noise when $d = \Omega(\log n)$.

This claim is made by combination of numerical result and analytical formula, and further supported from statistical physics argument. See discussions in Secs. IB, IIIC, IVD, Result 1, and Fig. 6 of the main text and Sec. III within the Supplemental Material [47].

Numerical result 1: our algorithm outperforms the experiments of Google and USTC for conventional random unitary circuits, that is, the single-qubit gate is Haar random.

See Secs. IB, IIIC, Result 2, Fig. 7, and Table I of the main text. See also Sec. V within the Supplemental Material [47] for more detail of our algorithm.

Numerical result 2: our algorithms achieve XEB value within around one order of magnitude of the experiments of Google and USTC for a slight modification of their gatesets.

See Secs. IB, IIIC, Result 3, Fig. 7, and Table I of the main text. See also Sec. V within the Supplemental Material [47] for more detail of our algorithm.

Numerical result 3: our algorithm exhibits favorable scaling behavior in increasing system sizes (while fixing the strength of noise and circuit depth) for both conventional gatesets and Google's gatesets.

See Secs. IB, IVC, and Fig. 2 of the main text and also Sec. II F within the Supplemental Material [47].

- [1] S. Arora and B. Barak, *Computational Complexity: a Modern Approach* (Cambridge University Press, Cambridge, United Kingdom, 2009).
- [2] S. Aaronson and A. Arkhipov, in *Proceedings of the forty-third annual ACM symposium on Theory of computing* (Association for Computing Machinery, New York NY USA, 2011), p. 333.
- [3] P. W. Shor, in *Proceedings 35th annual symposium on foundations of computer science* (Ieee, Santa Fe, NM, USA, 1994), p. 124.
- [4] J. Zhang, G. Pagano, P. W. Hess, A. Kyprianidis, P. Becker, H. Kaplan, A. V. Gorshkov, Z.-X. Gong, and C. Monroe, Observation of a many-body dynamical phase transition with a 53-qubit quantum simulator, Nature 551, 601 (2017).
- [5] F. Arute *et al.*, Quantum supremacy using a programmable superconducting processor, Nature **574**, 505 (2019).
- [6] Y. Wu et al., Strong quantum computational advantage using a superconducting quantum processor. arXiv preprint arXiv:2106.14734 (2021).
- [7] Q. Zhu *et al.*, Quantum computational advantage via 60-qubit 24-cycle random circuit sampling. arXiv preprint arXiv:2109.03494 (2021).
- [8] S. Ebadi et al., Quantum phases of matter on a 256atom programmable quantum simulator. arXiv preprint arXiv:2012.12281 (2020).
- [9] P. Scholl, Michael Schuler, Hannah J. Williams, Alexander A. Eberharter, Daniel Barredo, Kai-Niklas Schymik, Vincent Lienhard, Louis-Paul Henry, Thomas C. Lang, Thierry Lahaye, Andreas M. Läuchli, and Antoine

- Browaeys, Quantum simulation of 2D antiferromagnets with hundreds of Rydberg atoms, Nature **595**, 233 (2021), 2012.12268
- [10] J. Preskill, Quantum computing and the entanglement frontier. arXiv preprint arXiv:1203.5813 (2012).
- [11] A. W. Harrow and A. Montanaro, Quantum computational supremacy, Nature **549**, 203 (2017).
- [12] A. P. Lund, M. J. Bremner, and T. C. Ralph, Quantum sampling problems, bosonsampling and quantum supremacy, Npj Quantum Inf. 3, 1 (2017).
- [13] H.-S. Zhong *et al.*, Quantum computational advantage using photons, Science **370**, 1460 (2020).
- [14] H.-S. Zhong *et al.*, Phase-programmable Gaussian boson sampling using stimulated squeezed light, Phys. Rev. Lett. 127, 180502 (2021).
- [15] M. J. Bremner, R. Jozsa, and D. J. Shepherd, Classical simulation of commuting quantum computations implies collapse of the polynomial hierarchy, Proc. R. Soc. A: Mathematical, Physical and Engineering Sciences 467, 459 (2011).
- [16] M. J. Bremner, A. Montanaro, and D. J. Shepherd, Average-case complexity versus approximate simulation of commuting quantum computations, Phys. Rev. Lett. 117, 080501 (2016).
- [17] E. Farhi and A. W. Harrow, Quantum supremacy through the quantum approximate optimization algorithm. arXiv preprint arXiv:1602.07674 (2016).
- [18] S. Boixo, Sergei V. Isakov, Vadim N. Smelyanskiy, Ryan Babbush, Nan Ding, Zhang Jiang, Michael J. Bremner, John M. Martinis, and Hartmut Neven, Characterizing quantum supremacy in near-term devices, Nat. Phys. 14, 595 (2018).
- [19] M. J. Bremner, A. Montanaro, and D. J. Shepherd, Achieving quantum supremacy with sparse and noisy commuting quantum computations, Quantum 1, 8 (2017).
- [20] X. Gao, S.-T. Wang, and L.-M. Duan, Quantum supremacy for simulating a translation-invariant Ising spin model, Phys. Rev. Lett. **118**, 040502 (2017).
- [21] J. Bermejo-Vega, D. Hangleiter, M. Schwarz, R. Raussendorf, and J. Eisert, Architectures for quantum simulation showing quantum supremacy. arXiv preprint arXiv:1703.00466 (2017).
- [22] B. M. Terhal and D. P. DiVincenzo, Adaptive quantum computation, constant depth quantum circuits and arthurmerlin games. arXiv preprint arXiv:quant-ph/0205133 (2002).
- [23] S. Aaronson and L. Chen, Complexity-theoretic foundations of quantum supremacy experiments. arXiv preprint arXiv:1612.05903 (2016).
- [24] A. Bouland, B. Fefferman, C. Nirkhe, and U. Vazirani, On the complexity and verification of quantum random circuit sampling, Nat. Phys. 15, 159 (2019).
- [25] R. Movassagh, Efficient unitary paths and quantum computational supremacy: A proof of average-case hardness of random circuit sampling. arXiv preprint arXiv:1810.04681 (2018).
- [26] A. Bouland, B. Fefferman, Z. Landau, and Y. Liu, Noise and the frontier of quantum supremacy. arXiv preprint arXiv:2102.01738 (2021).
- [27] Y. Kondo, R. Mori, and R. Movassagh, Fine-grained analysis and improved robustness of quantum supremacy

- for random circuit sampling. arXiv preprint arXiv:2102.01960 (2021).
- [28] Since directly calculating the XEB value of 53-qubit Sycamore at depth 20 is computationally intractable, Google extrapolated their smaller-system results to estimate the final XEB value.
- [29] Y. Rinott, T. Shoham, and G. Kalai, Statistical aspects of the quantum supremacy demonstration. arXiv preprint arXiv:2008.05177 (2020).
- [30] A. Barenco, André Berthiaume, David Deutsch, Artur Ekert, Richard Jozsa, and Chiara Macchiavello, Stabilization of quantum computations by symmetrization, SIAM J. Comput. 26, 1541 (1997).
- [31] H. Buhrman, Richard Cleve, John Watrous, and Ronald de Wolf, Quantum fingerprinting, Phys. Rev. Lett. 87, 167902 (2001).
- [32] H. Huang, Richard Kueng, and John Preskill, Predicting many properties of a quantum system from very few measurements, Nat. Phys. 16, 1050 (2020).
- [33] The fidelity is closely related to the *Bhattacharyya coefficient* of two classical probability distributions.
- [34] C. Neill *et al.*, A blueprint for demonstrating quantum supremacy with superconducting qubits, Science **360**, 195 (2018).
- [35] J. Choi et al., Emergent randomness and benchmarking from many-body quantum chaos. arXiv preprint arXiv:2103.03535 (2021).
- [36] Y. Liu, M. Otten, R. Bassirianjahromi, L. Jiang, and B. Fefferman, Benchmarking near-term quantum computers via random circuit sampling. arXiv preprint arXiv:2105.05232 (2021).
- [37] S. Aaronson and S. Gunn, On the classical hardness of spoofing linear cross-entropy benchmarking. arXiv preprint arXiv:1910.12085 (2019).
- [38] J. Gray and S. Kourtis, Hyper-optimized tensor network contraction. arXiv preprint arXiv:2002.01935 (2020).
- [39] C. Huang et al., Classical simulation of quantum supremacy circuits. arXiv preprint arXiv:2005.06787 (2020).
- [40] F. Pan and P. Zhang, Simulating the sycamore quantum supremacy circuits. arXiv preprint arXiv:2103.03074 (2021).
- [41] H. Fu *et al.*, Closing the "quantum supremacy" gap: Achieving real-time simulation of a random quantum circuit using a new Sunway supercomputer. arXiv preprint arXiv:2110.14502 (2021).
- [42] X. Liu *et al.*, Redefining the quantum supremacy baseline with a new generation Sunway supercomputer. arXiv:2111.01066 (2021).
- [43] F. Pan, K. Chen, and P. Zhang, Solving the sampling problem of the Sycamore quantum supremacy circuits. arXiv:2111.03011 (2021).
- [44] The blog of Scott Aaronson. https://www.scottaaronson.com/blog/?p=5371 (2021).
- [45] C. L. Canonne, *A Survey on Distribution Testing: Your Data is Big. But is it Blue?* No. 9 in Graduate Surveys (Theory of Computing Library, 2020). http://www.theoryofcomputing.org/library.html.
- [46] I. L. Markov, A. Fatima, S. V. Isakov, and S. Boixo, Quantum supremacy is both closer and farther than it appears. arXiv preprint arXiv:1807.10749 (2018).

- [47] See Supplemental Material at http://link.aps.org/supplemental/10.1103/PRXQuantum.5.010334, which also includes Refs. [5,37,53,64,65,70,72,90–103].
- [48] The correction is roughly $1 + N\epsilon f(c)$ (see the Supplemental Material [47]). By assuming f(c) = 1, $N\epsilon \approx 0.25\%$.
- [49] Mathematically, we say p(x) and q(x) are uncorrelated if $\sum_{x} p(x)q(x)/2^{N} = (\sum_{x} p(x)/2^{N})(\sum_{x} q(x)/2^{N})$.
- [50] X. Mi et al., Information scrambling in quantum circuits, Science 374, 1479 (2021).
- [51] P. Hayden, Sepehr Nezami, Xiao-Liang Qi, Nathaniel Thomas, Michael Walter, and Zhao Yang, Holographic duality from random tensor networks, J. High Energy Phys. 2016, 9 (2016).
- [52] Y.-Z. You, Z. Yang, and X.-L. Qi, Machine learning spatial geometry from entanglement features, Phys. Rev. B 97, 045153 (2018).
- [53] N. Hunter-Jones, Unitary designs from statistical mechanics in random quantum circuits. arXiv preprint arXiv:1905. 12053 (2019).
- [54] T. Zhou and A. Nahum, Emergent statistical mechanics of entanglement in random unitary circuits, Phys. Rev. B 99, 174205 (2019).
- [55] C.-M. Jian, Y.-Z. You, R. Vasseur, and A. W. Ludwig, Measurement-induced criticality in random quantum circuits, Phys. Rev. B 101, 104302 (2020).
- [56] Y. Bao, S. Choi, and E. Altman, Theory of the phase transition in random unitary circuits with measurements, Phys. Rev. B 101, 104301 (2020).
- [57] J. Napp, R. L. La Placa, A. M. Dalzell, F. G. Brandao, and A. W. Harrow, Efficient classical simulation of random shallow 2D quantum circuits. arXiv preprint arXiv:2001.00021 (2019).
- [58] It is known that maximizing the (standard, nonlinear) cross-entropy is equivalent to minimizing the Kullback-Leibler divergence, which is a commonly used quantity for a statistical test of the closeness between the data and target distributions.
- [59] A. W. Harrow and R. A. Low, Random quantum circuits are approximate 2-designs, Commun. Math. Phys. 291, 257 (2009).
- [60] In realistic settings, one needs to distinguish the error rates associated with quantum gates and readout processes.
- [61] In order to implement the basic algorithm, we use a Julia package for quantum circuit simulation, cuyao: https://yaoquantum.org.
- [62] In order to implement the self-averaging algorithm, we use another julia package for tensor network contraction, omeinsum https://under-peter.github.io/OMEinsum.jl/dev/.
- [63] G. Kalachev, P. Panteleev, and M.-H. Yung, Recursive multi-tensor contraction for XEB verification of quantum circuits. arXiv preprint arXiv:2108.05665 (2021).
- [64] Y. Zhou, E. M. Stoudenmire, and X. Waintal, What limits the simulation of quantum computers?, Phys. Rev. X 10, 041038 (2020).
- [65] A. Harrow and S. Mehraban, Approximate unitary *t*-designs by short random quantum circuits using nearest-neighbor and long-range gates. arXiv preprint arXiv:1809.06957 (2018).
- [66] X. Gao and L. Duan, Efficient classical simulation of noisy quantum computation. arXiv preprint arXiv:1810.03176 (2018).

- [67] B. Barak, C.-N. Chou, and X. Gao, in 12th Innovations in Theoretical Computer Science Conference (ITCS 2021), (2021), p. 30:1, 2005.02421.
- [68] K. Huang, Statistical Mechanics (John Wiley & Sons., New York, 10 1963).
- [69] C. Dankert, R. Cleve, J. Emerson, and E. Livine, Exact and approximate unitary 2-designs and their application to fidelity estimation, Phys. Rev. A **80**, 012304 (2009).
- [70] M.-D. Choi, Completely positive linear maps on complex matrices, Linear Algebra Appl. 10, 285 (1975).
- [71] In this work, we focus on the experimentally relevant regime, where the strength of noise and the depth of the circuit are not too large, such that the fidelity remains sufficiently greater than 2^{-N} . When the fidelity is close to 2^{-N} , the discussion in this paragraph no longer holds, as the contribution from subdominant terms in Eq. (26) becomes significant.
- [72] A. M. Dalzell, N. Hunter-Jones, and F. G. Brandão, Random quantum circuits anti-concentrate in log depth. arXiv preprint arXiv:2011.12277 (2020).
- [73] D. Hangleiter, M. Kliesch, J. Eisert, and C. Gogolin, Sample complexity of device-independently certified "quantum supremacy", Phys. Rev. Lett. **122**, 210502 (2019).
- [74] J. Emerson, R. Alicki, and K. Życzkowski, Scalable noise estimation with random unitary operators, J. Opt. B: Quantum Semiclassical Opt. 7, S347 (2005).
- [75] E. Knill, D. Leibfried, R. Reichle, J. Britton, R. B. Blakestad, J. D. Jost, C. Langer, R. Ozeri, S. Seidelin, and D. J. Wineland, Randomized benchmarking of quantum gates, Phys. Rev. A 77, 012307 (2008).
- [76] T. J. Proctor, Arnaud Carignan-Dugas, Kenneth Rudinger, Erik Nielsen, Robin Blume-Kohout, and Kevin Young, Direct randomized benchmarking for multiqubit devices, Phys. Rev. Lett. 123, 030503 (2019).
- [77] S. Kimmel, M. P. da Silva, C. A. Ryan, B. R. Johnson, and T. Ohki, Robust extraction of tomographic information via randomized benchmarking, Phys. Rev. X 4, 011050 (2014).
- [78] J. Wallman, C. Granade, R. Harper, and S. T. Flammia, Estimating the coherence of noise, New J. Phys. 17, 113020 (2015).
- [79] J. Helsen, X. Xue, L. M. Vandersypen, and S. Wehner, A new class of efficient randomized benchmarking protocols, Npj Quantum Inf. 5, 1 (2019).
- [80] A. Erhard, Joel J. Wallman, Lukas Postler, Michael Meth, Roman Stricker, Esteban A. Martinez, Philipp Schindler, Thomas Monz, Joseph Emerson, and Rainer Blatt, Characterizing large-scale quantum computers via cycle benchmarking, Nat. Commun. 10, 1 (2019).
- [81] R. Harper, S. T. Flammia, and J. J. Wallman, Efficient learning of quantum noise, Nat. Phys. 16, 1184 (2020).
- [82] D. Koller and N. Friedman, Probabilistic Graphical Models: Principles and Techniques (MIT press, Cambridge, MA, USA, 2009).
- [83] D. Niedermayer, in *Innovations in Bayesian networks: Theory and applications* (Springer, Berlin, Heidelberg, 2008), p. 117.
- [84] A. Deshpande *et al.*, Tight bounds on the convergence of noisy random circuits to uniform. arXiv preprint arXiv:2112.00716 (2021).

- [85] J. Eisert, Dominik Hangleiter, Nathan Walk, Ingo Roth, Damian Markham, Rhea Parekh, Ulysse Chabaud, and Elham Kashefi, Quantum certification and benchmarking, Nat. Rev. Phys. 2, 382 (2020).
- [86] G. D. Kahanamoku-Meyer, S. Choi, U. V. Vazirani, and N. Y. Yao, Classically-verifiable quantum advantage from a computational Bell test. arXiv preprint arXiv:2104.00687 (2021).
- [87] Z. Brakerski, V. Koppula, U. Vazirani, and T. Vidick, Simpler proofs of quantumness. arXiv preprint arXiv:2005. 04826 (2020).
- [88] Z. Liu and A. Gheorghiu, Depth-efficient proofs of quantumness. arXiv preprint arXiv:2107.02163 (2021).
- [89] S. Hirahara and F. L. Gall, Test of quantumness with small-depth quantum circuits. arXiv preprint arXiv:2105.05500 (2021).
- [90] Jacob C. Bridgeman and Christopher T. Chubb, Handwaving and interpretive dance: An introductory course on tensor networks, J. Phys. A: Math. Theor. 50, 223001 (2017).
- [91] John Watrous, The Theory of Quantum Information (Cambridge University Press, Cambridge, United Kingdom, 2018).
- [92] Don Weingarten, Asymptotic behavior of group integrals in the limit of infinite rank, J. Math. Phys. 19, 999 (1978).
- [93] Paolo Zanardi, Christof Zalka, and Lara Faoro, Entangling power of quantum evolutions, Phys. Rev. A 62, 030301 (2000).
- [94] Farrokh Vatan and Colin Williams, Optimal quantum circuits for general two-qubit gates, Phys. Rev. A (2004).
- [95] Steven R. White, Density matrix formulation for quantum renormalization groups, Phys. Rev. Lett. **69**, 2863 (1992).
- [96] Guifré Vidal, Efficient classical simulation of slightly entangled quantum computations, Phys. Rev. Lett. **91**, 142902 (2003).
- [97] Frank Verstraete, Valentin Murg, and J. Ignacio Cirac, Matrix product states, projected entangled pair states, and variational renormalization group methods for quantum spin systems, Adv. Phys. 57, 143 (2008).
- [98] Sebastian Paeckel, Thomas Köhler, Andreas Swoboda, Salvatore R. Manmana, Ulrich Schollwöck, and Claudius Hubig, Time-evolution methods for matrix-product states, Ann. Phys. 411, 167998 (2019).
- [99] Daniel Greenbaum, Introduction to quantum gate set tomography. arXiv preprint arXiv:1509.02921 (2015).
- [100] Benoît Collins, Moments and cumulants of polynomial random variables on unitarygroups, the Itzykson-Zuber integral, and free probability, Int. Math. Res. Not. **2003**, 953 (2003).
- [101] Benoît Collins and Piotr Śniady, Integration with respect to the Haar measure on unitary, orthogonal and symplectic group, Commun. Math. Phys. 264, 773 (2006).
- [102] Rodney J. Baxter, Exactly Solved Models in Statistical Mechanics (Elsevier, Amsterdam, Netherlands, 2016).
- [103] Fernando GSL Brandao, Aram W. Harrow, and Michał Horodecki, Local random quantum circuits are approximate polynomial-designs, Commun. Math. Phys. 346, 397 (2016).